AR-010-666

Synchronous Averaging of Helicopter Tail Rotor Gearbox Vibration: Phase Reference Considerations

D.M. Blunt

DSTO-TR-0739

APPROVED FOR PUBLIC RELEASE

© Commonwealth of Australia

DEPARTMENT OF DEFENCE
DEFENCE SCIENCE AND TECHNOLOGY ORGANISATION

Synchronous Averaging of Helicopter Tail Rotor Gearbox Vibration: Phase Reference Considerations

D.M. Blunt

Airframes and Engines Division
Aeronautical and Maritime Research Laboratory

DSTO-TR-0739

ABSTRACT

Synchronous averaging requires an accurate phase reference (tachometer) signal. In helicopter transmissions, such a signal can usually be obtained or derived from an engine or main rotor gearbox accessory, but is not as readily available for the tail rotor gearbox. This report examines whether a separate tail rotor gearbox phase reference signal is necessary by investigating the relative jitter, due to dynamic tail drive shaft twist, between phase reference signals obtained from the main and tail rotor gearboxes in a S-70A-9 Black Hawk helicopter.

19990308 161

RELEASE LIMITATION

Approved for public release

DEPARTMENT OF DEFENCE

DEFENCE SCIENCE AND TECHNOLOGY ORGANISATION

DTIC QUALITY INSPECTED 1

AQF99-06-1124

Published by

DSTO Aeronautical and Maritime Research Laboratory
PO Box 4331
Melbourne Victoria 3001 Australia

Telephone: (03) 9626 7000
Fax: (03) 9626 7999
© Commonwealth of Australia 1998
AR-010-666
October 1998

APPROVED FOR PUBLIC RELEASE

Synchronous Averaging of Helicopter Tail Rotor Gearbox Vibration: Phase Reference Considerations

Executive Summary

Synchronous averaging is a signal processing technique that significantly enhances the ability to detect and diagnose faults in rotating machinery by 'extracting' the vibration for a particular shaft from the overall gearbox vibration. It is based on the principle that the forced vibration of a shaft, and the components attached to and rotating with it, will be periodic with the shaft rotation. The technique requires an accurate phase reference to synchronise the sampling of the vibration signal with the rotational frequency of the shaft. The synchronous samples are then divided into segments of one rotational period, and ensemble-averaged to attenuate the non-synchronous frequencies.

Because it is often difficult to obtain a phase reference signal directly from a helicopter tail rotor gearbox, this investigation was conducted to determine whether such a direct signal was necessary, or if an indirect phase reference signal from the main rotor gearbox would be sufficient. The investigation focused on the possibilty for dynamic twisting of the long tail drive shaft, and how this might produce phase errors at the tail rotor shaft. These errors, even if very small, have the potential to significantly reduce the sensitivity of fault detection methods based on the synchronous averaging process.

The data from a recent flight trial in an Australian Army S-70A-9 Black Hawk helicopter were analysed to determine:

a) the relative differences between main and tail phase reference signals, and
b) the effect of these differences on the synchronous averages of the tail gearbox output shaft vibration.

It was found that during forward flight the dynamic twisting of the tail drive shaft appears to be minimised, but that during hover, and particularly tail rotor turns, there appears to be a significant amount of twisting. This was found to produce a consequential degradation of the synchronous averages.

It was also discovered that, in the S-70A-9, forward flight induces undesirable vibration impulses into the tail gearbox vibration signal. These have subsequently been confirmed to exist in the S-70B-2 as well. The cause of the impulses is speculated to be the aerodynamic interaction of the main rotor tip vortices on the tail rotor blades. The impulses are undesirable from a vibration analysis point of view because of their potential to mask faults within the gearbox.

It is therefore recommended that:

a) a direct phase reference signal from the tail rotor gearbox should always be used, and
b) S-70/H-60 series tail rotor gearbox vibration should only be analysed during hover.

These recommendations have a direct outcome for the AMRL-developed transmission vibration monitoring system currently being implemented in all Royal Australian Navy S-70B-2 Seahawk and SK-50 Sea King helicopters. This system consists of vibration transducers hard-wired into the aircraft, and a carry-on/carry-off data acquisition/analysis unit. Tail rotor photocells are being fitted to both types of helicopters, and tail rotor gearbox vibration data will only be acquired during hover out of ground effect.

Authors

David Blunt
Airframes and Engines Division

Mr Blunt graduated from the University of Western Australia in 1989 with a Bachelor of Engineering degree with first class honours in Mechanical Engineering. He joined the Aeronautical and Maritime Research Laboratory in 1990 and has been working in the field of helicopter gearbox fault detection since 1992. Mr Blunt has been involved with a number of in-flight and test cell trials conducted on fixed and rotary wing aircraft transmissions operated by the Australian Defence Force.

Contents

1. Introduction

Synchronous averaging is a technique regularly employed in the analysis of helicopter transmission vibration to provide estimates of the vibration from individual shafts and their associated components. It is fundamentally based on the principle that the forced vibration of a shaft, and the components fixed to and rotating with it (eg gears), will be periodic with the shaft rotation.[1] Synchronous averaging requires an accurate shaft phase reference (tachometer) signal to divide the gearbox vibration signal into periods of exactly one shaft revolution. These segments are then ensemble-averaged to attenuate the non-synchronous components. The resultant average is treated as if it were the time-domain vibration signal for one revolution of the isolated shaft with its attached components.

As would be expected, synchronous averaging is very dependent on the accuracy of the phase reference signal. Any phase jitter, or error, in this signal will make the synchronous vibration appear slightly non-synchronous, and cause it to be attenuated during the averaging process.

Since gearbox shafts are kinematically linked by their gear ratios, a single phase reference signal will usually be sufficient to synchronously average the vibration of all the gearbox shafts. The use of this signal may also be extended to external drivetrain components, but the further the components are from the location of the phase reference, the more likely it is for the flexibility of the drive system to introduce additional phase errors. This will be even more likely if the drivetrain is subject to torque fluctuations. These additional phase errors will be superimposed on top of those inherent in the phase reference signal, and degrade the synchronous average even further.

In helicopter transmissions, the gearboxes that will be most susceptible to this phenomenon are those at the end of the long tail drive shaft: that is, the tail rotor gearbox and, if it exists, the intermediate gearbox at the base of the tail pylon. This is because phase reference signals can usually be obtained, or derived, from an engine or main rotor gearbox accessory, such as an AC generator, but are not readily available for the intermediate or tail rotor gearboxes. It should also be noted that, in most helicopters, the tail drive shaft is typically made of three or four shorter shafts. These are supported by hanger bearings mounted in soft viscous dampers, and connected by flexible couplings, both of which may contribute to the overall flexibility of the shaft.

To investigate this potential problem, a photocell was fitted to the tail rotor of an Australian Army S-70A-9 Black Hawk helicopter during a recent trial installation of a transmission vibration monitoring system [1]. This supplemented a phase reference signal derived from an AC generator geared into the main rotor transmission. Data

[1] This excludes rolling element bearings because of slip.

were captured under a number of different flight conditions, and the relative phase jitter between the two signals was examined by:

a) calculating the difference in tail rotor phase angle derived from each signal, and
b) comparing the synchronous averages of the tail rotor gearbox output shaft computed using each signal.

2. Theory

A brief description of synchronous averaging is presented below. For a more detailed examination, particularly on the effects of various interpolation methods on the digital re-sampling of vibration data, the reader is referred to Forrester [2]. This description is followed by a simple mathematical model of the attenuation effect of reference phase jitter on a synchronous average.

2.1 Synchronous Averaging

The synchronous averaging process for a continuous vibration signal is illustrated in Figure 1. Note that the tachometer must be of type that gives a reference phase angle (e.g. a pulse at a specific shaft angle); a tachometer that simply gives a voltage proportional to speed is not suitable.

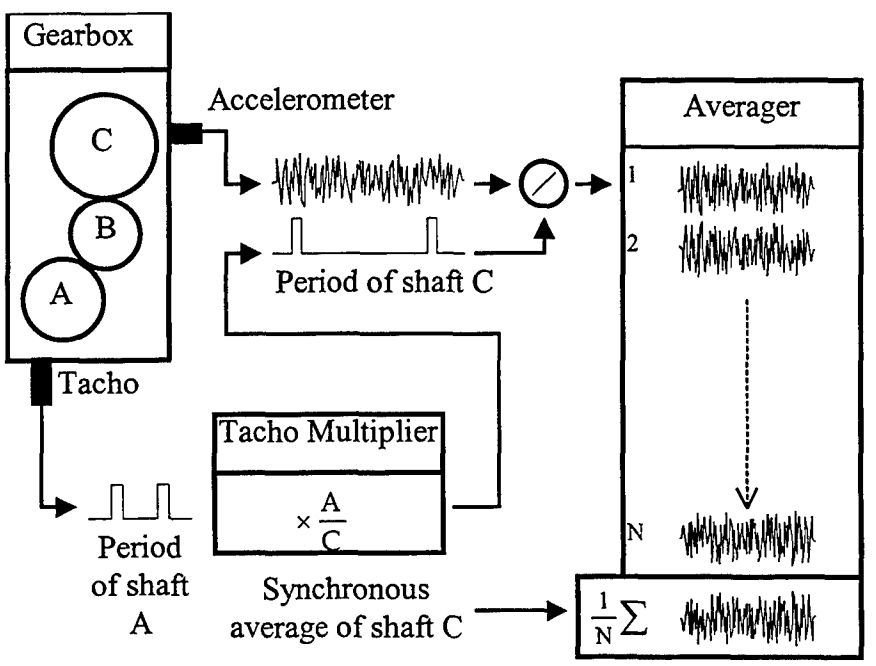

Figure 1. Synchronous Averaging.

In practice, synchronous averaging is usually implemented within a digital computer using discretely sampled vibration and phase reference signals. This therefore requires

a mechanism to ensure the vibration data are sampled at equally spaced angular increments of the shaft of interest. That is, if P samples are required for each revolution of the shaft of interest, then the sample rate in the angle-domain must be $P/2\pi$ for that shaft, regardless of any perturbations in shaft speed. The technique used at AMRL to accomplish this is described below.

2.1.1 AMRL Synchronous Averaging Technique

1. The vibration and reference phase signals are simultaneously sampled at a rate that is sufficient to avoid aliasing, and provide at least as many samples per revolution of the shaft of interest as required.

2. The equivalent cumulative phase angles of the data are calculated by:
   a) searching the phase reference data for the zero-crossings (these are linearly interpolated between the points on either side of the zero-crossing level[2]); and
   b) linearly interpolating the phase angle of each sample between the zero-crossings.

3. The vibration data are then digitally re-sampled with fifth order splines, using the cumulative phase angle results to provide the re-sampling positions. Fifth order splines have been shown to be as good as ideal low-pass filters when reconstructing a signal from data with a dynamic range less than 75 dB (eg from a 12-bit A-D converter) [2].

4. The re-sampled data are then split into segments corresponding to one rotation period of the shaft of interest, and ensemble-averaged.

2.2 Effect of Reference Phase Jitter

The synchronous averaging process can be modelled in the angle-domain by the following equation:

$$\bar{x}(\theta) = \frac{1}{N}\sum_{n=0}^{N-1} x(\theta + n2\pi) \qquad 1$$

where:

x is the vibration signal,
θ is the shaft angle of the averaged vibration signal over the period $[0,2\pi]$, and
N is the number of shaft revolutions averaged.

If for each shaft angle, θ, the reference phase jitter angle, ϕ, is modelled as a random variable, then Equation 1 can be expressed as:

$$\bar{x}(\theta) = \frac{1}{N}\sum_{n=0}^{N-1} x(\theta + n2\pi + \phi_\theta(n)) \qquad 2$$

---

[2] The zero-crossing level need not necessarily be zero Volts. In the data examined here, a level mid way between the minimum and maximum values of the phase reference signal was used.

It is intuitive that, for a particular level of phase jitter, the higher frequencies of the synchronous average will be attenuated more than the lower frequencies. This relationship can be determined by taking the Fourier Transform of Equation 2.

$$\begin{aligned}\bar{X}(\gamma) &= \int\left[\frac{1}{N}\sum_{n=0}^{N-1} x(\theta + n2\pi + \phi_\theta(n))\right] e^{-j\gamma\theta}\, d\theta \\ &= \int\left[\frac{1}{N}\sum_{n=0}^{N-1}\left(\int X(f) e^{jf(\theta+n2\pi+\phi_\theta(n))} df\right)\right] e^{-j\gamma\theta}\, d\theta \\ &= \frac{1}{N}\sum_{n=0}^{N-1}\iint X(f) e^{jf(\theta+n2\pi+\phi_\theta(n))}\, e^{-j\gamma\theta}\, df\, d\theta\end{aligned} \qquad 3$$

where:

X is the Fourier Transform of x, and

γ is the frequency in shaft orders (cycles / shaft cycle).

If the phase jitter variable is now assumed to be uniform across all shaft angles (ie is independent of θ), Equation 3 becomes:

$$\begin{aligned}\bar{X}(\gamma) &= \frac{1}{N}\sum_{n=0}^{N-1}\iint X(f) e^{jf(n2\pi+\phi(n))}\, e^{j(f-\gamma)\theta}\, df\, d\theta \\ &= \frac{1}{N}\sum_{n=0}^{N-1}\int X(f) e^{jf(n2\pi+\phi(n))}\, \delta(f-\gamma)\, df \\ &= X(\gamma)\frac{1}{N}\sum_{n=0}^{N-1} e^{j\gamma(n2\pi+\phi(n))}\end{aligned} \qquad 4$$

where:

δ is the Dirac delta function.

It can be seen from Equation 4 that the summation is the combined effect of synchronous averaging and phase jitter on the Fourier Transform of the vibration. At the non-synchronous frequencies the summation will approach zero (ie where $\gamma \neq$ integer), while at the synchronous frequencies:

$$e^{j\gamma n2\pi} = 1 \quad , \gamma \text{ an integer}$$

The attenuation factor, A, of the synchronous frequency components is therefore:

$$A(\gamma) = \frac{1}{N}\sum_{n=0}^{N-1} e^{j\gamma\phi(n)} \quad , \gamma \text{ an integer} \qquad 5$$

By dropping the requirement for γ to be an integer, Equation 5 will instead represent the envelope of the attenuation factor. In the limit as $N \to \infty$, this becomes:

$$\mathrm{A}(\gamma) = \int_{-\infty}^{+\infty} \mathrm{P}[\phi] e^{j\gamma\phi}\, d\phi \qquad 6$$

where $\mathrm{P}[\phi]$ is the probability density function of ϕ.

If the jitter is assumed to have a normal distribution with zero mean and standard deviation σ, Equation 6 becomes:

$$A(\gamma) = \int_{-\infty}^{\infty} \left(\frac{1}{\sigma\sqrt{2\pi}} e^{-\left(\frac{\phi^2}{2\sigma^2}\right)} \right) e^{j\gamma\phi}\, d\phi \qquad 7$$

$$= e^{\frac{-1}{2}(\sigma\gamma)^2}$$

Since, in practice, N will be finite, the actual attenuation factor can be expected to lie in some band about Equation 7. Since the difference between the actual attenuation factor and Equation 7 can be interpreted as a variation in the standard deviation of the jitter, the statistical confidence interval for σ can be used to place confidence limits on this band. The confidence interval for σ [3] is given by

$$\left[\sigma\sqrt{\frac{N-1}{\chi^2_{\frac{\alpha}{2};N-1}}},\ \ \sigma\sqrt{\frac{N-1}{\chi^2_{1-\frac{\alpha}{2};N-1}}} \right]$$

where:

N	number of revolutions averaged,
$100(1-\alpha)$	is the percentage confidence interval, and
χ^2	denotes the chi-square distribution with N-1 degrees of freedom.

For example, if N = 101, the 99% confidence interval for the standard deviation, σ, would be

$$\left[\sigma\sqrt{\frac{100}{140.169}},\ \ \sigma\sqrt{\frac{100}{67.328}} \right] = \left[0.8446\sigma,\ \ 1.2187\sigma \right]$$

and, as N increases, the interval will become smaller. This is illustrated in Figure 2, where Equation 7 is plotted for various σ, and the 95% confidence bands for N = 101 and N = 399[3] are shaded about each curve.

Note, however, that without an absolute phase reference, as is the case in this investigation (since both signals can be expected to have some inherent level of phase jitter), Equation 7 cannot be used to determine the absolute attenuation of each synchronous average. The ratio of attenuation factors, however, can be expressed as:

[3] This is the value of N used for the synchronous averages of the tail rotor gearbox output shaft discussed in the later sections.

$$\frac{A_1(\gamma)}{A_2(\gamma)} = \frac{e^{\frac{-1}{2}(\sigma_1\gamma)^2}}{e^{\frac{-1}{2}(\sigma_2\gamma)^2}} \qquad 8$$

$$= e^{\frac{-1}{2}\gamma^2\left(\sigma_1^2-\sigma_2^2\right)}$$

That is, the ratio of the attenuation factors has the same form as the individual factors (as long as $\sigma_1 > \sigma_2$), with the variance replaced by the difference in variance.

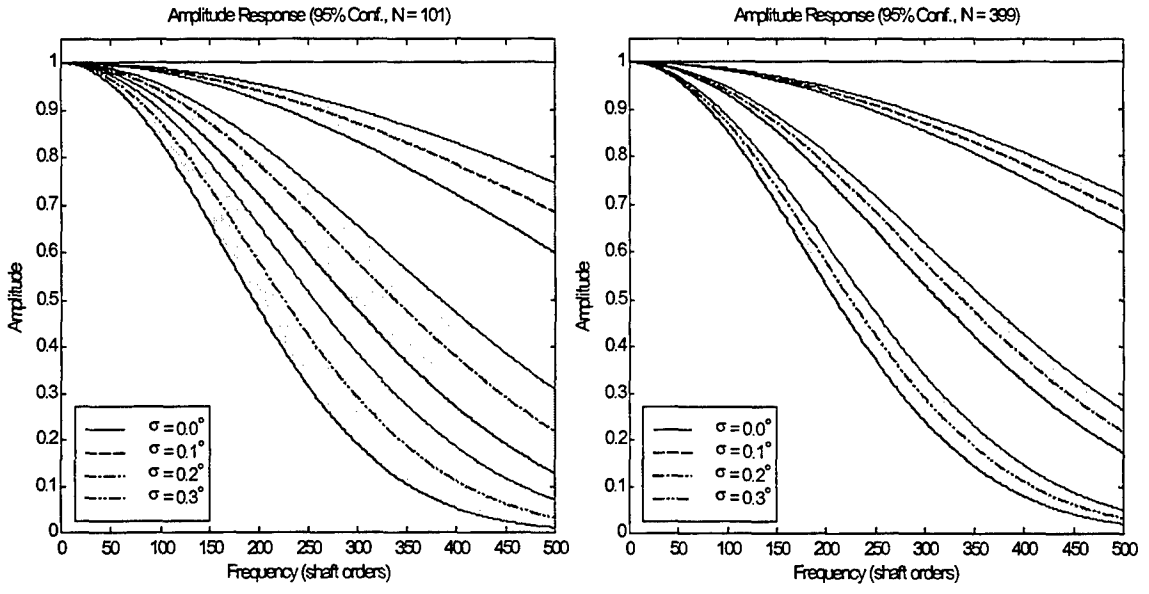

Figure 2. Attenuation Factor for Various Levels of Normally Distributed Reference Phase Jitter with Shaded 95% Confidence Bands, for N=101 and N=399.

3. AMRL Transmission Vibration Monitoring System

3.1 S-70A-9 Transmission

The S-70A-9 transmission is shown in Figure 3. The individual shaft speeds and gear mesh frequencies are listed in Appendix 1. The transmission consists of:

a) two input modules that are driven by the engines at power turbine speed (~20,900 rpm);
b) two accessory modules that drive the hydraulic pumps and electrical generators;
c) a main module that drives the main rotor and the tail drive shaft;
d) an intermediate gearbox at the base of the tail pylon; and
e) a tail rotor gearbox at the top of the tail pylon.

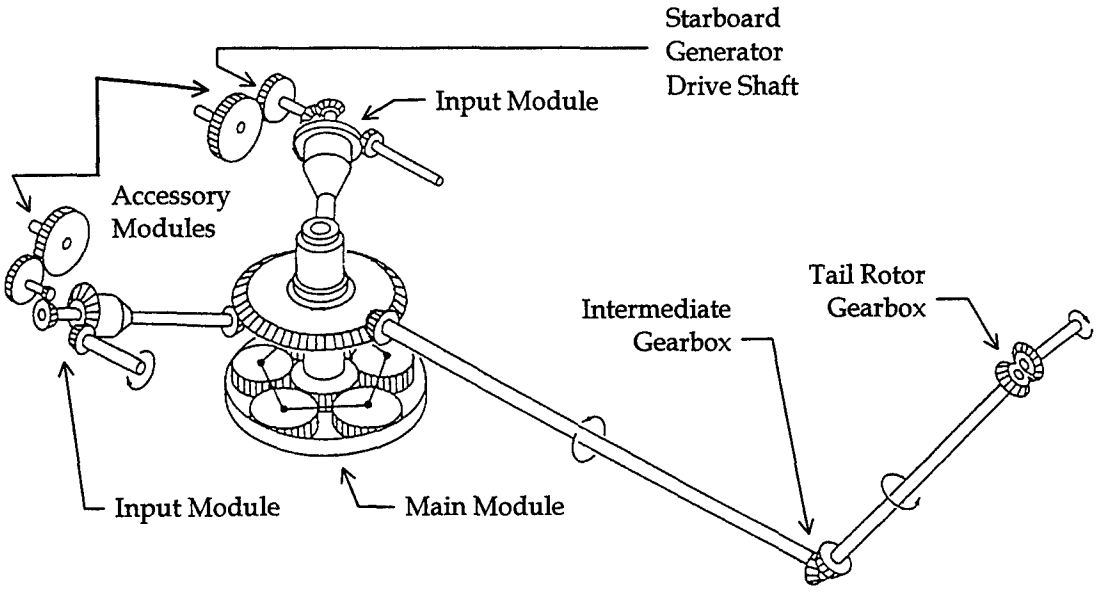

Figure 3. S-70A-9 Transmission.

3.2 System Hardware

The AMRL-developed transmission vibration monitoring system is shown schematically in Figure 4. It consists of:

a) a portable ruggedised computer with internally mounted signal conditioning, anti-alias filtering, and analogue-to-digital converter cards;
b) a connector interface on the side of the computer;
c) accelerometers mounted on the transmission modules/gearboxes;
d) a tail rotor photocell and photocell processor; and
e) cables to connect the computer to the transducers and aircraft power.

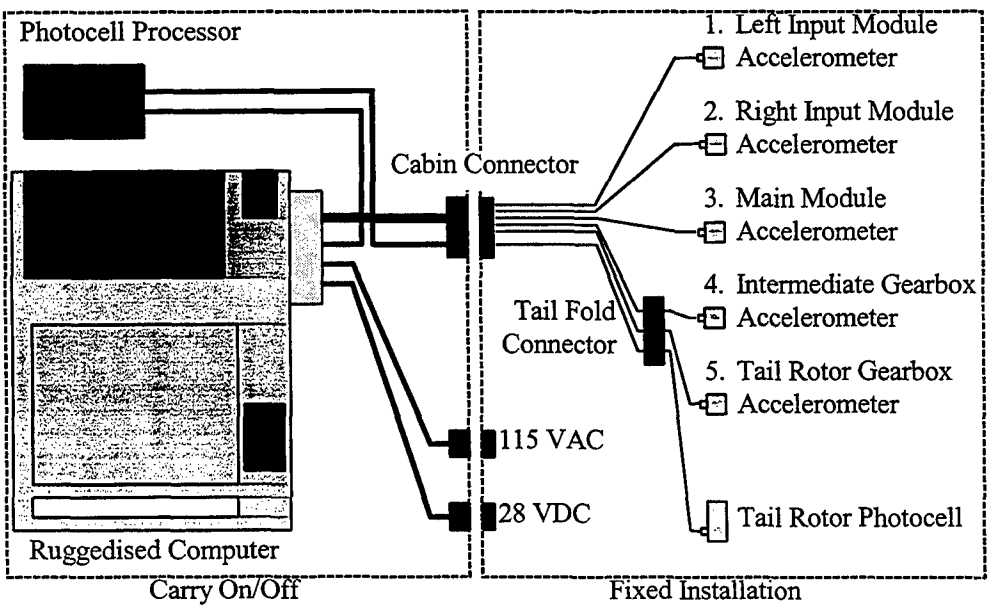

Figure 4. Transmission Vibration Monitoring System.

3.3 Phase Reference Signals

3.3.1 Main Transmission

Since the AC generators are directly driven by the accessory gearbox modules (see Figure 3), a single phase of the 115 VAC power supply can be used as a phase reference signal for the main transmission. Due to the construction of the generator, the supply frequency is exactly twice its shaft speed. Thus, although the transmission is kept at a 'constant' speed by the engine controllers, any perturbation in speed will have a corresponding perturbation in the supply frequency. From the data examined in this report, the average supply frequency was calculated to be approximately 395 Hz.

The signal from the AC generator was obtained from a power receptacle in the cabin roof. This receptacle normally receives power from the starboard generator. The amplitude of the signal was attenuated from 115 VAC to approximately 4 VAC by a resistor network on the signal conditioning card.

3.3.2 Tail Rotor

The tail rotor phase reference signal was obtained from a photocell and photocell processor (Chadwick-Helmuth Parts 10200 & 10170) obtained from a rotor track and balance kit. The photocell was mounted on top of the tail pylon approximately 480 mm behind the centre-line of the tail rotor shaft. It was pointed directly at the tail rotor disc with a slight declination (approx. 15° below the horizontal) to reduce interference from direct sunlight. A piece of reflective tape approximately 20 mm x 50 mm was fixed to the inner leading edge of one of the tail rotor blades. The beam length was approximately 275 mm.

The 10 V sharp edged pulses from the photocell processor were reduced to approximately 1.7 V by a resistor network on the signal conditioning card. The pulse frequency was approximately 20 Hz.

4. Flight Data

4.1 Data Acquisition

Data from the two phase reference signals and the tail rotor gearbox vibration signal were simultaneously acquired using the parameters listed in Table 1 for each of the flight conditions listed in Table 2.

Table 1. Data Acquisition Parameters.

Channels	Tail rotor gearbox accelerometer, Photocell signal, and AC Generator signal	
Total Sample Rate	42,105.26 Hz (4.00 MHz ±0.01% clock / 95)	
Sample Rate / Channel	14,035.09 Hz	
Acquisition Period	22 s	
Anti-alias Filter	Tail rotor accelerometer Photocell signal AC Generator signal	5,000 Hz Bypass Bypass

Table 2. Flight Conditions.

#	Flight Condition	Altitude (ft)	KIAS	Engine Torque (%/%)	Nr (%)
A	Straight & Level 60%	1300	110	60/60	100
B	Straight & Level 70%	1300	120	70/70	100
C	Straight & Level 80%	1100	125	80/80	100
D	Straight & Level 90%	1100	135	90/90	100
E	Straight & Level 100%	1100	140	100/100	100
F	Right Turn - 30° Bank	1300	120	80/80	100
G	Right Turn - 45° Bank	1300	120	80/80	100
H	Hover	25	0	60/60	100
I	Clockwise Tail Rotor Turn	25	0	60/60	100
J	Anti-clockwise Tail Rotor Turn	25	0	60/60	100

4.2 Data Processing

The raw data files were first processed with AMRL software, and the results were then analysed using MATLAB (see Appendix 2 for the M files), as described below.

4.2.1 Raw Data

For each flight condition:

1. The equivalent cumulative phase angles of the data were calculated (see §2.1.1).
2. A separate synchronous average (see Table 3) of the tail rotor gearbox output shaft vibration was calculated using the each of the two different phase reference data records.

Table 3. Synchronous Average Parameters for Tail Rotor Gearbox Output Shaft

Re-sample Rate (Samples/Rev)	Shaft Revs Averaged	Ratio of Shaft to AC Generator Signal	Ratio of Shaft to Photocell Signal
1024	399[4]	1/2 × 37/76 × 21/100 * 75/22 × 25/31 × 19/53 = 1107225 / 21976768	1 / 1

[4] Chosen as a multiple of the number of teeth on the mating pinion (19) to minimise the modulation of the output gear average by the input pinion.

4.2.2 Rotor Speed Perturbations

While the main rotor speed in the Black Hawk is nominally constant (the engines are controlled to a constant speed), it is inevitable that load fluctuations will induce small perturbations about this speed. Since a constant speed implies that the phase angle should increase linearly, these perturbations can be examined by subtracting a straight line fit from the cumulative phase data. To enable the same fit to be used for both data series, the AC generator data were first converted to tail rotor phase angle units by:

a) multiplying the AC generator data by the gear ratio between the generator and the tail rotor (1107225/21976768),
b) performing a linear regression on the data using the MATLAB *polyfit* and *polyval* functions,
c) subtracting this linear fit from both signals, and
d) removing any offset between the data series by subtracting their means.

4.2.3 Relative Phase Difference

The relative difference (jitter) between the cumulative phase data were examined by converting the AC generator data into tail rotor phase angle units, then subtracting these data from the photocell data, and estimating the probability density function of the difference. This was done by:

a) multiplying the AC generator data by the gear ratio between the generator and the tail rotor (1107225/21976768),
b) subtracting the AC generator data from the photocell data,
c) removing any zero-offset of the difference data by subtracting the mean,
d) converting the difference data to degrees, and
e) calculating a histogram of the difference data using the MATLAB *hist* function.

4.2.4 Synchronous Average Difference

To compare the synchronous averages, they were first aligned to remove any phase offset[5], then the AC generator average was subtracted from the photocell average. This was done by:

a) finding the phase angle corresponding to the point of maximum (circular) cross-correlation between the averages, using the MATLAB *fmin* function,
b) phase-shifting the AC generator average by this angle, and
c) subtracting the phase-shifted AC generator average from the photocell average.

[5] The phase offsets between the synchronous averages were an artefact of the averaging process, which was arbitrarily started at the first zero-crossing of the respective phase reference signals.

5. Results

The results from the rotor speed perturbations, relative phase difference, probability density function estimates, and synchronous average difference analyses are presented below.

5.1 Rotor Speed Perturbations

The effects of rotor speed perturbations on the tail rotor phase angle are shown from Figure 5 to Figure 14 (see §4.2.2 for description of method). The vertical axis shows the deviation of the tail rotor angle from that which would be expected if the tail rotor speed was exactly constant. In each figure, the plot on the left shows the entire data record, while the plot on the right shows a selected segment.

The following observations can be made about these figures:

1. The rotor speed perturbations during forward flight (straight and level, and banked turns) are smaller than those during hover flight (hover, and tail rotor turns). This is evidence of larger torque variations during hover, probably caused by the pilot trying to maintain station at a fixed point over the ground.

2. On the macro scale, the left hand plots reveal virtually no detectable separation between the photocell and AC generator phase data, showing that both signals seem to follow each other very well, which is as would be expected for a geared drivetrain.

3. On the micro scale, however, the right hand plots reveal that there are detectable differences between the phase data which can be characterised by their flight conditions.
   a) Forward flight: The photocell data appears to have a small degree of "overshoot" compared to the AC generator data. It can be seen that where the curves change direction, corresponding to an acceleration or deceleration of the rotors, the AC generator data responds before the photocell data. This is probably because the phase angles are calculated with a zero-crossing algorithm (see §2.1.1), and the AC generator signal has a higher frequency than the photocell signal (395 Hz compared to 20 Hz).
   b) Hover Flight: In these cases, there are larger and longer separations between the photocell and AC generator data. While this may still be partially attributable to the "overshoot" mentioned above, the sustained separation of the data is more likely to be due to twisting of the long tail drive shaft caused by variation of the tail rotor torque. The presence and the characteristic duration of these deviations is consistent with pedal control movements made by the pilot, which would be expected to be greater during hover and tail rotor turns, than in forward flight.

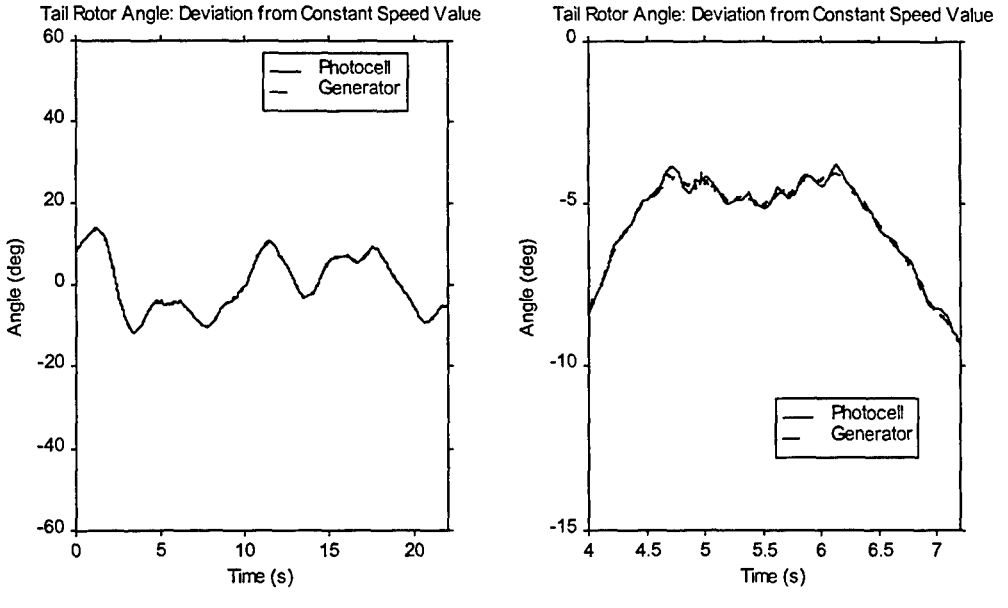

Figure 5. Effect of Rotor Speed Perturbations on the Tail Rotor Phase Angle for Straight and Level Flight, 60% Torque.

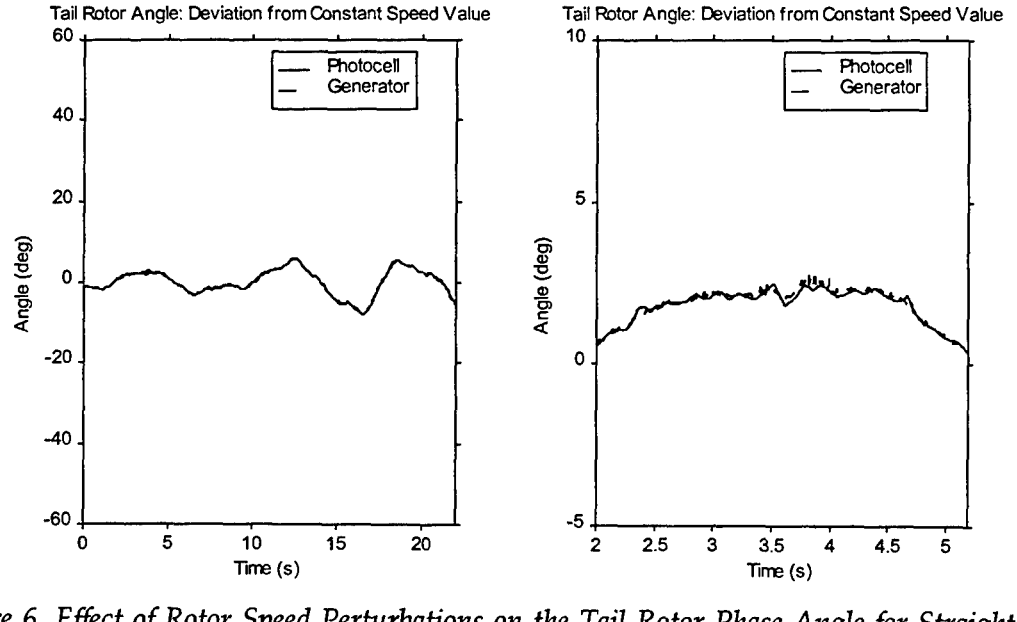

Figure 6. Effect of Rotor Speed Perturbations on the Tail Rotor Phase Angle for Straight and Level Flight, 70% Torque.

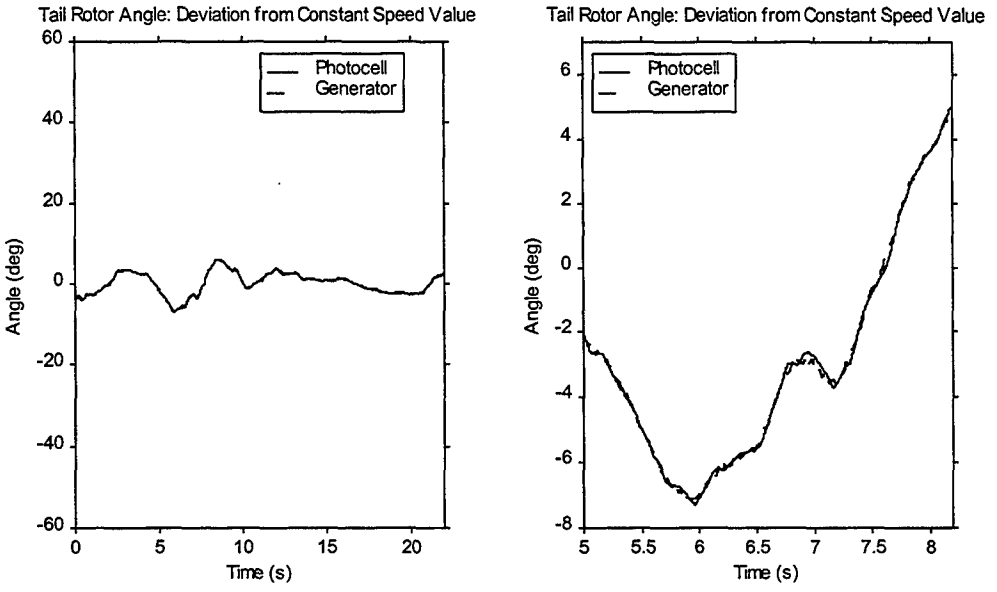

Figure 7. Effect of Rotor Speed Perturbations on the Tail Rotor Phase Angle for Straight and Level Flight, 80% Torque.

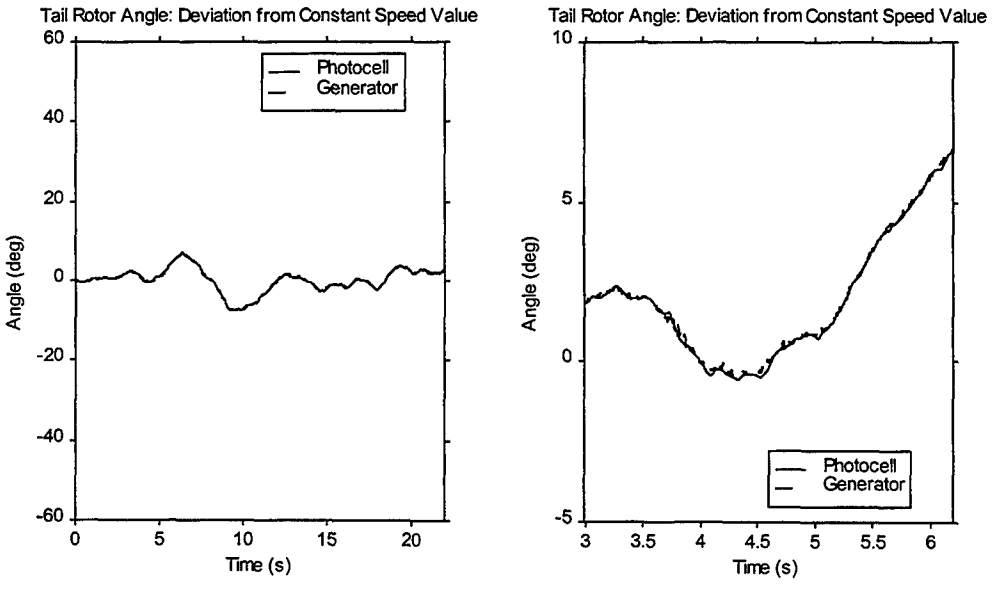

Figure 8. Effect of Rotor Speed Perturbations on the Tail Rotor Phase Angle for Straight and Level Flight, 90% Torque.

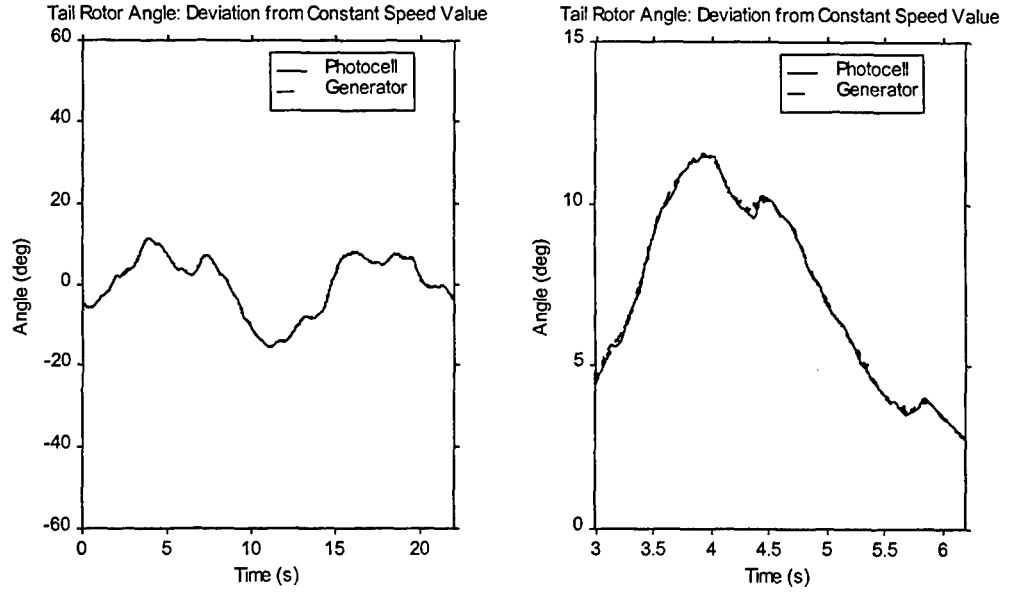

Figure 9. Effect of Rotor Speed Perturbations on the Tail Rotor Phase Angle for Straight and Level Flight, 100% Torque.

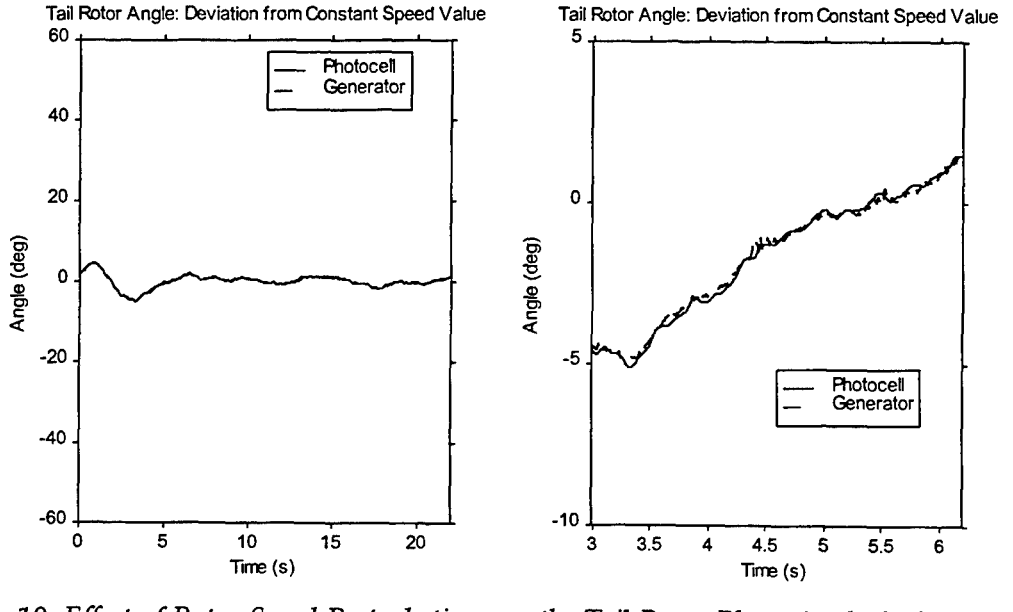

Figure 10. Effect of Rotor Speed Perturbations on the Tail Rotor Phase Angle for Right Turn, 30° Bank.

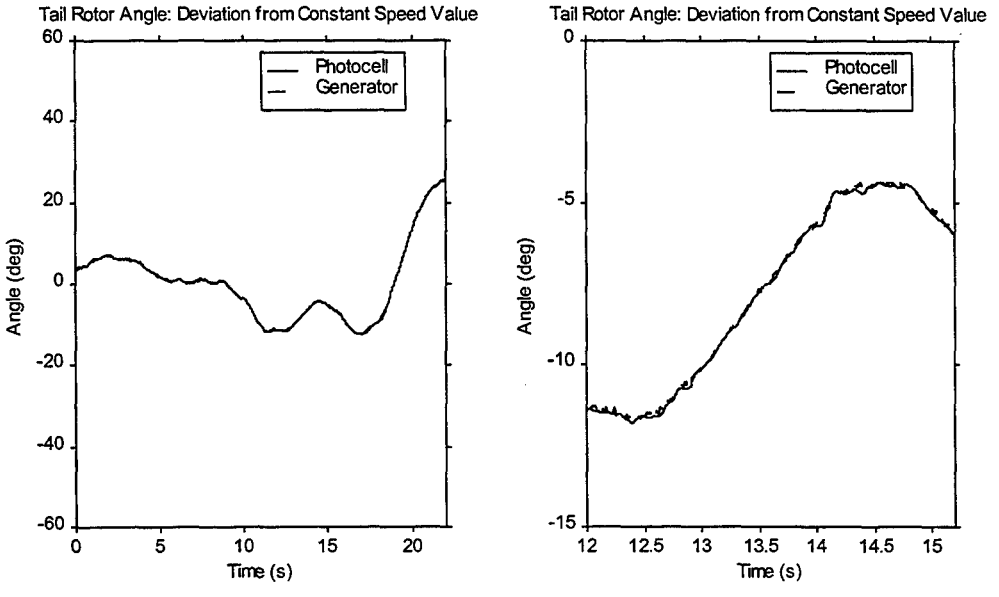

Figure 11. Effect of Rotor Speed Perturbations on the Tail Rotor Phase Angle for Right Turn, 45° Bank.

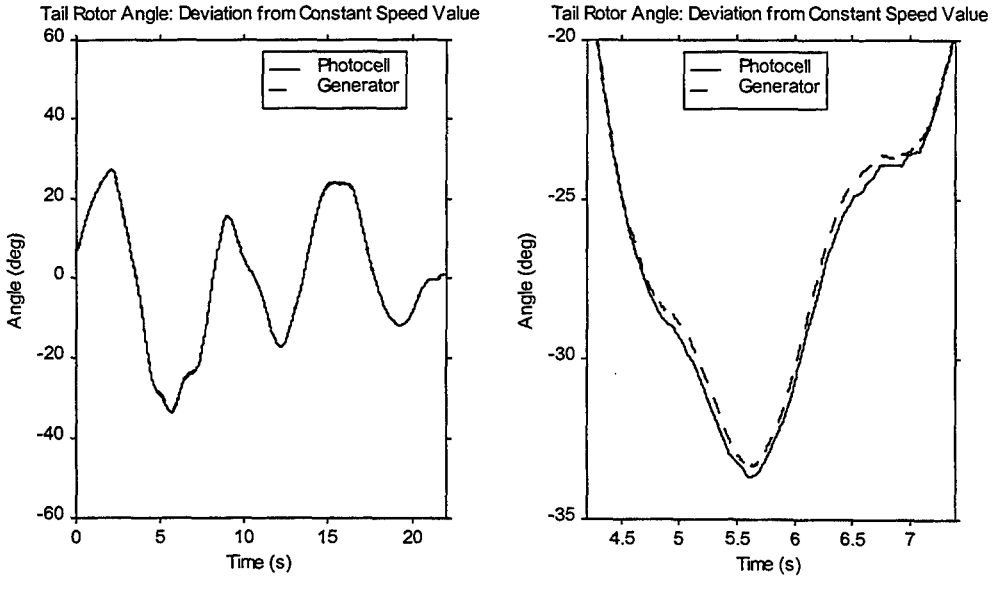

Figure 12. Effect of Rotor Speed Perturbations on the Tail Rotor Phase Angle for Hover.

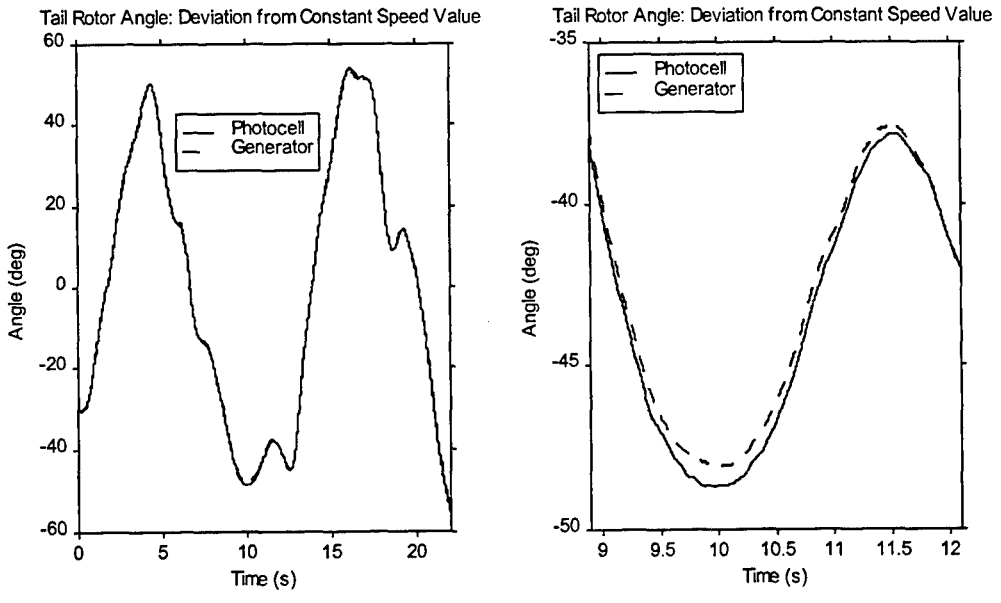

Figure 13. Effect of Rotor Speed Perturbations on the Tail Rotor Phase Angle for Clockwise Tail Rotor Turn.

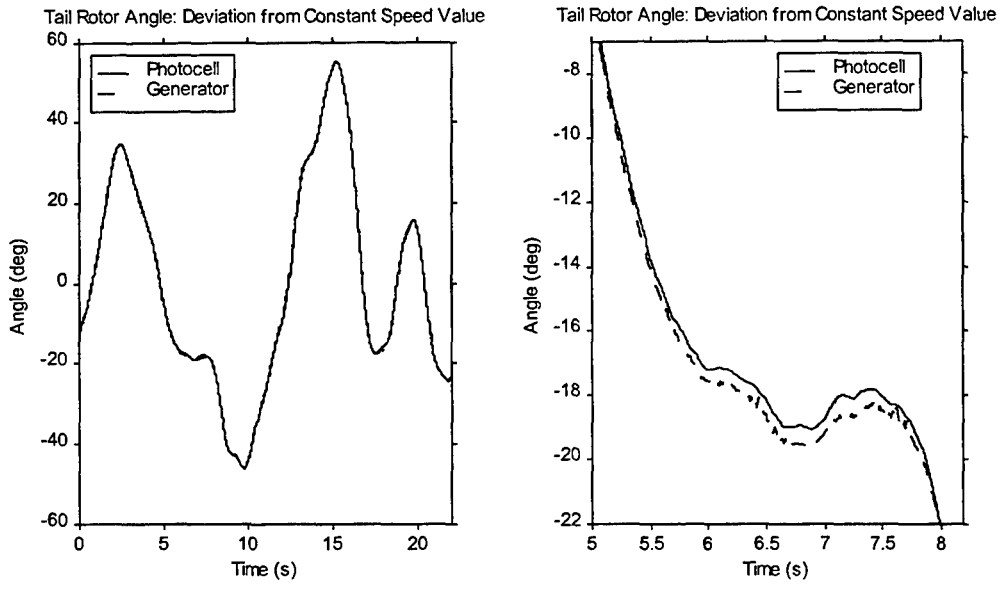

Figure 14. Effect of Rotor Speed Perturbations on the Tail Rotor Phase Angle for Anti-Clockwise Tail Rotor Turn.

5.2 Relative Phase Difference

The relative differences between the two tail rotor phase data sets for each flight condition (obtained by subtracting one data set from the other) are shown from Figure 15 to Figure 24. The most distinguishing feature of these plots is the disparity between results for the forward flight and hover flight conditions. Apart from the seemingly random high frequency 'noise' present in the forward flight results, these plots are

relatively flat, with only a few underlying deviations evident beneath the noise. On the other hand, the hover flight results exhibit quite large underlying deviations. Generally, these features correlate well with the phase separations observed in §5.1. From this, it is postulated that, in general:

a) the underlying large scale deviations correspond to the dynamic twisting of the tail drive shaft brought about by pilot induced tail rotor torque variations, and
b) the 'noise' is most probably attributable to measurement error (see §5.5).

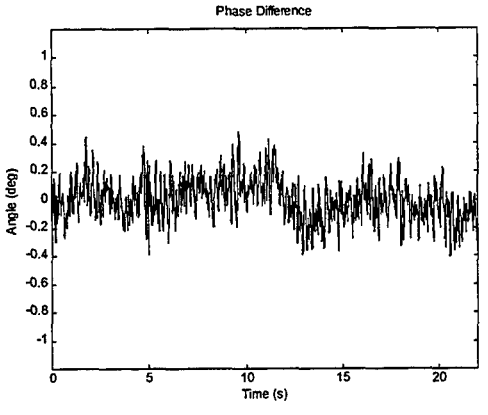

Figure 15. Relative Phase Difference for Straight & Level Flight, 60% Torque.

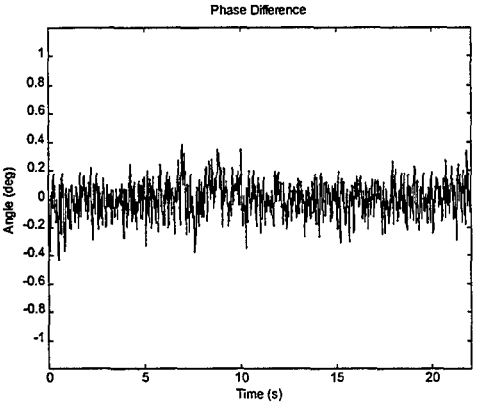

Figure 17. Relative Phase Difference for Straight & Level Flight, 80% Torque.

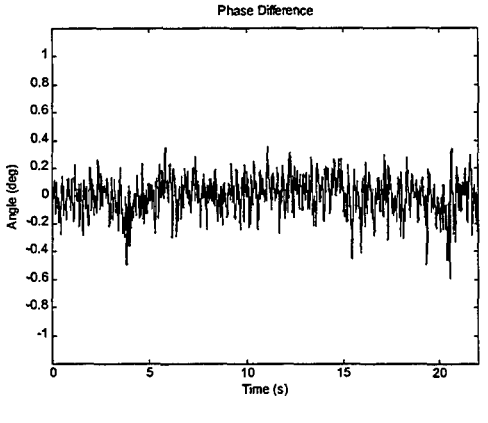

Figure 16. Relative Phase Difference for Straight & Level Flight, 70% Torque.

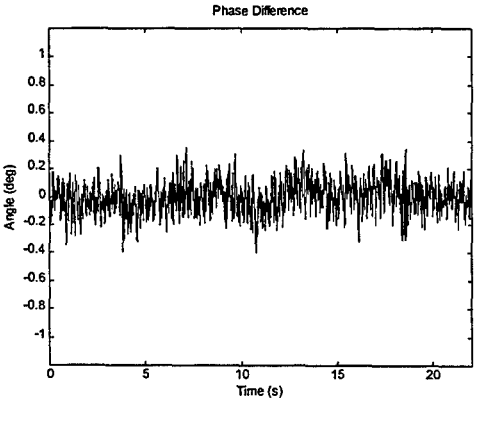

Figure 18. Relative Phase Difference for Straight & Level Flight, 90% Torque.

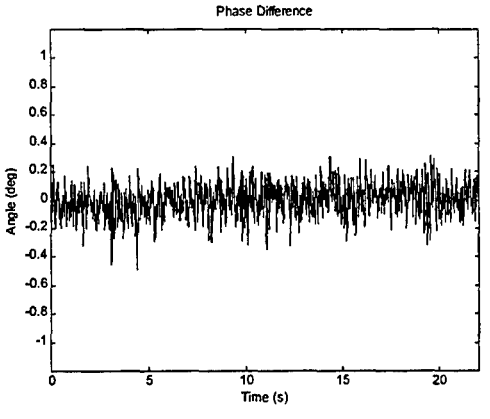

Figure 19. Relative Phase Difference for Straight & Level Flight, 100% Torque.

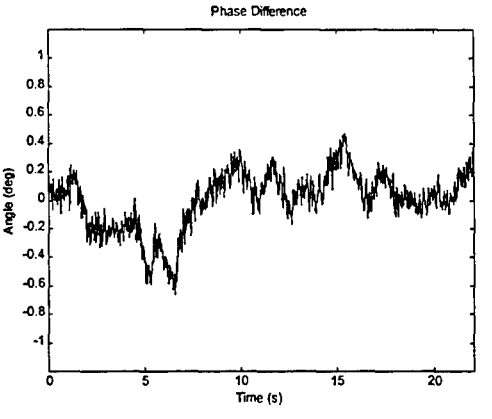

Figure 22. Relative Phase Difference for Hover.

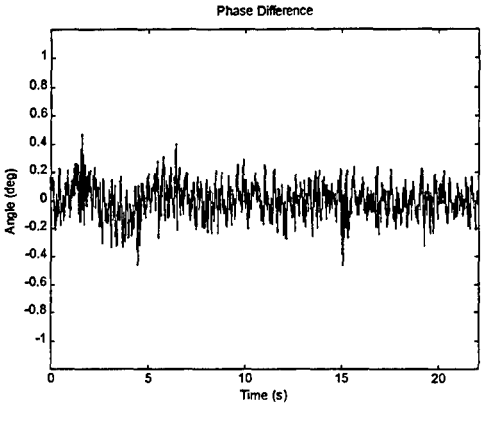

Figure 20. Relative Phase Difference for Right Turn, 30° Bank.

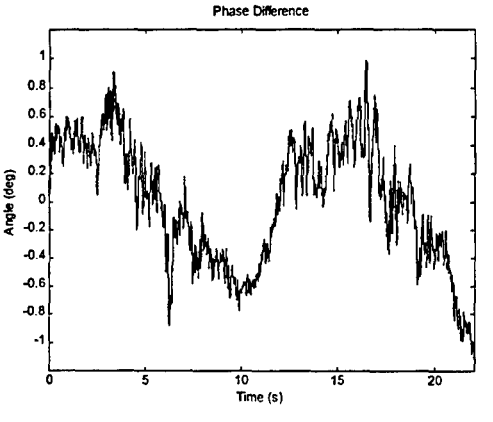

Figure 23. Relative Phase Difference for Clockwise Tail Rotor Turn.

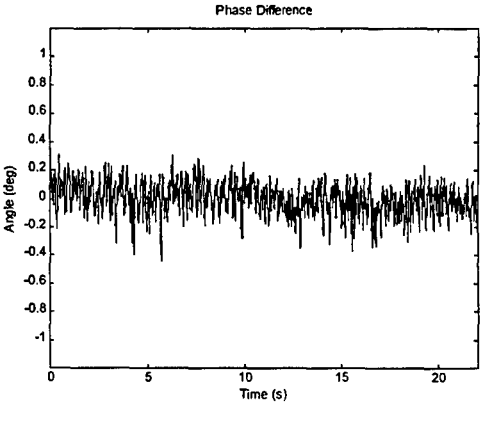

Figure 21. Relative Phase Difference for Right Turn, 45° Bank.

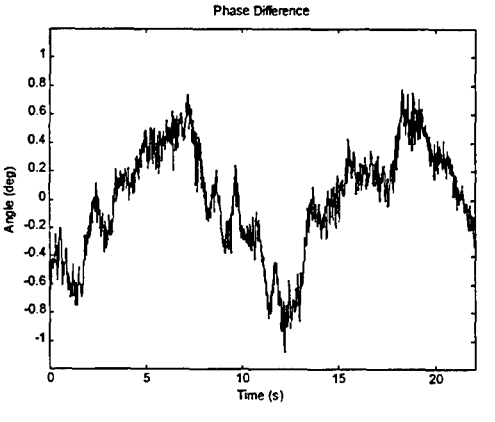

Figure 24. Relative Phase Difference for Anti-Clockwise Tail Rotor Turn.

5.3 Probability Density Function Estimates

The probability density function (PDF) estimates of the relative phase difference data from §5.2 are shown from Figure 25 to Figure 34. They were calculated across a band from -1.33° to 1.33°, with 133 bins of width 0.020°. The standard deviation, minimum and maximum are shown in the upper right corner of each plot. For comparison, a normal distribution with the same standard deviation has been overlaid on top of each PDF.

It can be seen from these plots that the distinguishing features previously identified in the phase difference data (see §5.2) are directly translated into their probability density functions. The plots can therefore be split into the same two groups: forward flight, and hover flight. The following observations can be made about these two groups.

5.3.1 Forward Flight

1. Each PDF estimate very closely approximates the overlaid normal distribution. The small departures from the normal distribution curve can be attributed to the small underlying deviations evident in the corresponding figures of §5.2. Note, however, that even though the difference data approach a normal distribution, this does not necessarily imply that the underlying jitter inherent in each phase reference signal is also normally distributed, although it is likely.

2. The standard deviations of the distributions decrease slightly with engine torque, from 0.139° at 60% torque, to 0.102° at 100% torque. This would appear to correlate well with the magnitude of the underlying deviations observed in the corresponding figures of §5.2. From this, and the postulation that they were caused by tail rotor torque variation, it can be inferred that this decreases slightly as the forward airspeed increases (from 110 to 140 KIAS).

5.3.2 Hover Flight

1. These distributions do not match the overlaid normal distributions. The large departures from the normal curve can be attributed to the large underlying deviations caused by the dynamic tail drive shaft twist evident in the corresponding figures of §5.2.

2. The standard deviations of the distributions increase for the tail rotor turns, from 0.204° for hover, to 0.441° for the clockwise turn, and 0.383° for the anticlockwise turn. This is probably due to the pilot making larger pedal adjustments during the tail rotor turns, than while hovering.

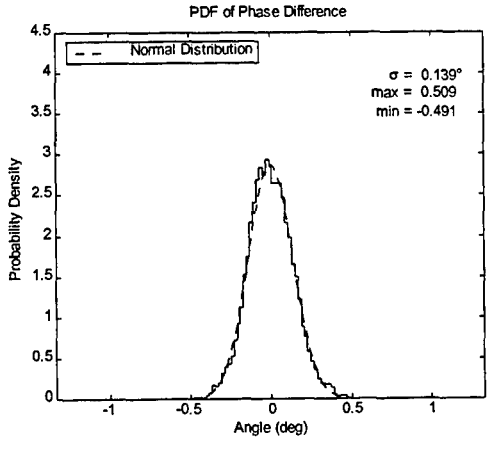

Figure 25. PDF Estimate of Phase Difference for Straight & Level Flight, 60% Torque.

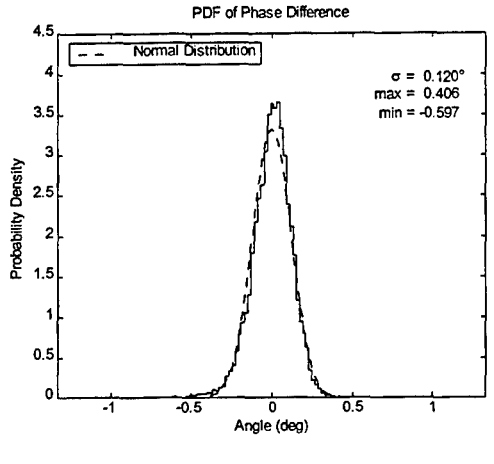

Figure 26. PDF Estimate of Phase Difference for Straight & Level Flight, 70% Torque.

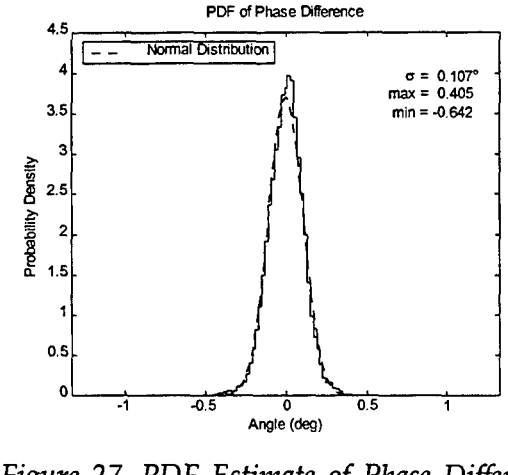

Figure 27. PDF Estimate of Phase Difference for Straight & Level Flight, 80% Torque.

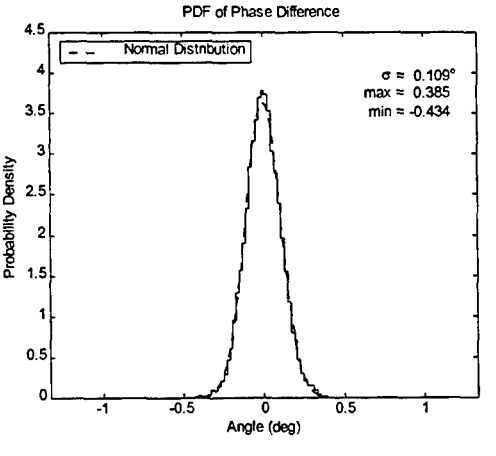

Figure 28. PDF Estimate of Phase Difference for Straight & Level Flight, 90% Torque.

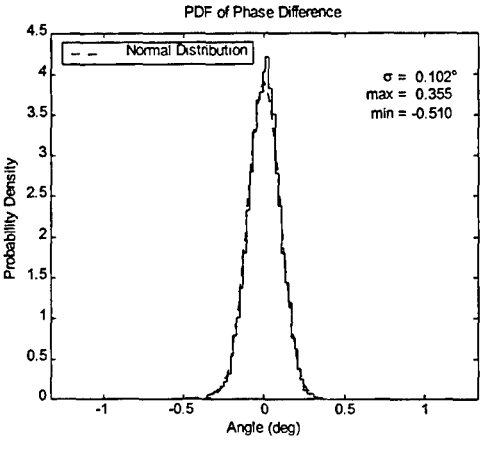

Figure 29. PDF Estimate of Phase Difference for Straight & Level Flight, 100% Torque.

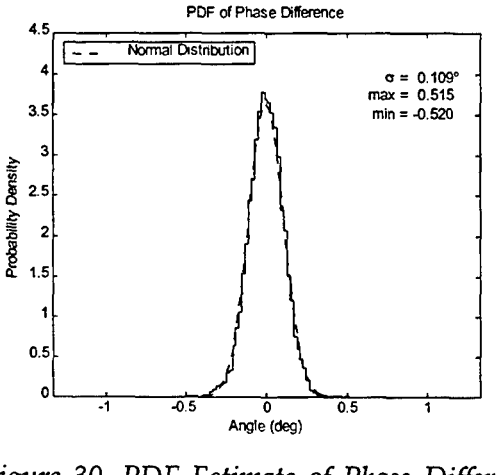

Figure 30. PDF Estimate of Phase Difference for Right Turn, 30° Bank.

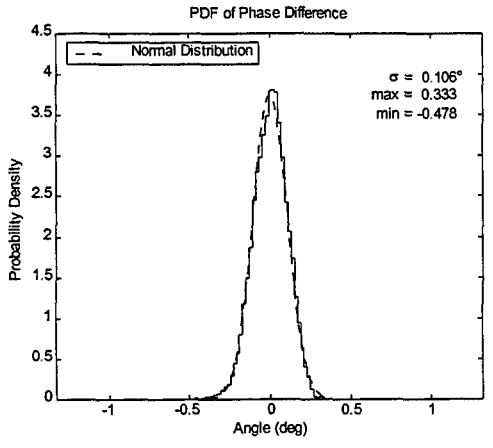

Figure 31. PDF Estimate of Phase Difference for Right Turn, 45° Bank.

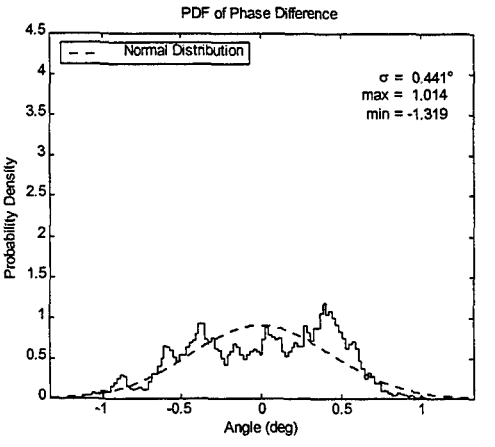

Figure 33. PDF Estimate of Phase Difference for Clockwise Tail Rotor Turn.

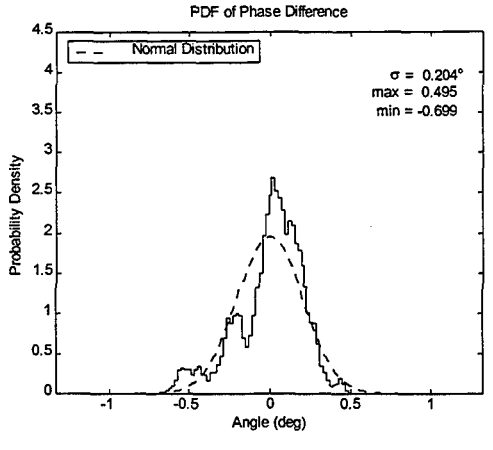

Figure 32. PDF Estimate of Phase Difference for Hover.

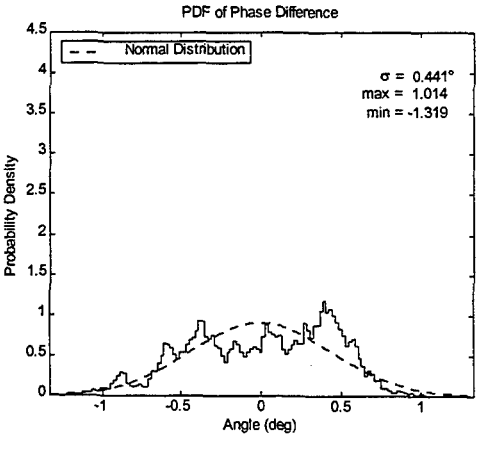

Figure 34. PDF Estimate of Phase Difference for Anti-Clockwise Tail Rotor Turn.

5.4 Synchronous Averages

The synchronous averages of the tail rotor gearbox output shaft vibration are shown from Figure 39 to Figure 48. Each figure is split into three sections showing:

a) the synchronous average and its spectrum computed using the photocell signal,
b) the synchronous average and its spectrum computed using the AC generator signal, and
c) the difference between the synchronous averages, and the amplitude ratios of the gear mesh harmonics.

For comparison purposes, the signal amplitudes have been extracted from these figures and summarised in Table 4.

Before discussing these results, however, the following information in §5.4.1 and §5.4.2 should be noted.

5.4.1 Attenuation due to Reference Phase Jitter

The theoretical attenuation of a synchronous average due to reference phase jitter was developed in §2.2. Application of this theory to the data, however, is limited by two factors:

1. Firstly, there is no absolute measure of the phase jitter in each phase reference signal, as both must be considered to have at least some measurement error (see §5.5). Also, the tail rotor photocell signal cannot automatically be assumed to provide a more accurate measure of the tail rotor angle than the AC generator signal. In fact, the higher frequency of the AC generator signal (395 Hz), compared to the photocell signal (20 Hz), may allow it to better follow any short term speed perturbations (disregarding dynamic shaft twisting) (see §5.1).

   Without an absolute phase reference, the absolute attenuation of the synchronous vibration frequencies cannot be determined. All that can be examined is the ratio of the attenuation factors. From Equation 8, this was shown to have the same form as the individual attenuation factors for each average (as long as $\sigma_1 > \sigma_2$), but with the jitter variance replaced by the difference in jitter variance. If the assumptions made in deriving Equation 8 hold, then the amplitude ratios of the gear mesh harmonics should follow the general shape of the curves shown in Figure 2.

2. Secondly, as can be seen in §5.3, the assumption in §2.2 of normally distributed phase jitter is not necessarily valid for any of the data examined here. It would appear that the measurement error component of the jitter comes close to being normally distributed, but the tail drive shaft twist component does not. Attempts were made to separate the measurement error from the underlying dynamic tail drive shaft twist (so that they might be investigated separately) by filtering the data, but this was unsuccessful because no matter where the cross-over frequency was placed, some of the measurement error would be left mixed in with the shaft twist, and vice versa.

   Since the assumption of normally distributed phase jitter does not necessarily apply, the amplitude ratios of the gear mesh harmonics cannot be expected to follow exactly the curves shown in Figure 2. The more the jitter departs from a normal distribution, the more the amplitude ratios can be expected to depart from these curves.

5.4.2 Extraneous Vibration Impulses

Large impulses were observed in the tail rotor gearbox vibration data for all the forward flight conditions, but not during the hover flight conditions. An example of these impulses is shown in Figure 35, with the detail of a typical impulse shown in Figure 36. Although impulses are typically symptomatic of a loose accelerometer, this

was found not to be the case. It is therefore speculated that, since the impulses only occurred during forward flight, they were probably caused by the aerodynamic interaction between the tail rotor blades and the main rotor tip vortices. That is, during forward flight, the main rotor tip vortices were being swept back through the tail rotor disc, and wherever they intersected with a tail rotor blade they would generate a shock in the blade that would travel through the hub to the gearbox. During hover the vortices would descend vertically away from the main rotor and not interact with the tail rotor. If this speculation is correct, then the impulses are not desirable for health monitoring because they may mask faults within the gearbox.

It is difficult to determine the extent to which the impulses have affected the synchronous averages shown here. As the impulses were slightly non-synchronous, they have been attenuated by the averaging process, leaving little visual evidence of their presence in the averages. This is not to say that their effects have been entirely removed, however, as their presence alone has forced the expansion of the ADC input range, effectively reducing dynamic range of the gear mesh vibration data. For the purposes of this investigation, however, any remaining effects should not affect comparisons between the averages greatly, since the same vibration data were used for each average.

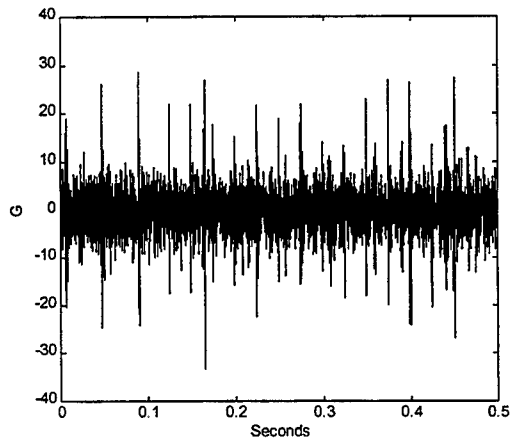

Figure 35. Typical Tail Rotor Gearbox Vibration During Forward Flight.

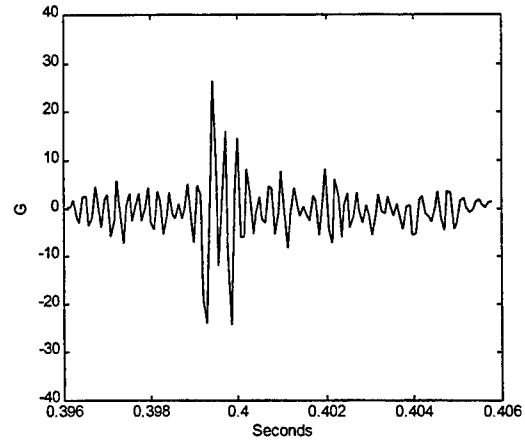

Figure 36. Typical Impulse.

5.4.3 Forward Flight

The following observations can be made about the forward flight synchronous averages.

1. In general, and especially when compared to hover flight (see §5.4.4), there is good overall agreement between the AC generator and photocell averages. This indicates that where dynamic twisting of the tail drive shaft is minimised, both phase reference signals perform similarly well for synchronous averaging purposes.

2. It can be seen from Table 4, however, that the overall amplitudes of the AC generator averages are, in all but one case (flight condition E - 100% torque), slightly larger than the photocell averages. This indicates, in a general sense, that the AC generator may provide a fractionally more accurate phase reference signal in these flight conditions than the photocell, probably because of its higher frequency and lack of "overshoot" (see §5.1). These differences are quite small, however, and do not necessarily justify the preferential selection of the AC generator signal over the photocell signal.

3. The amplitudes of the gear mesh harmonics (multiples of 53 shaft orders) in the AC generator averages are nearly all slightly greater than, or equal to, those in the photocell averages. This provides some additional evidence that the AC generator signal might be a fractionally better phase reference than the photocell signal. It should be noted, however, that the amplitude ratios, plotted in Figure 37, for the first four gear mesh harmonics are all very close to a value of one, which is the expected ratio for phase reference signals with equal levels of jitter (see §5.4.1). These results therefore also show some qualitative agreement with the mathematical model. The larger amplitude variations for the fifth harmonic may be caused by this frequency falling in the transition-band of the anti-alias filter, as small changes in rotor speed will have affected the attenuation of this frequency differently to the other harmonics (due to the slope of the filter response).

5.4.4 Hover Flight

The following observations can be made about the hover flight synchronous averages.

1. In general, there is poor overall agreement between the AC generator and photocell averages. This indicates that the dynamic tail drive shaft twist observed in §5.2 has a very significant effect on the synchronous averaging of the tail rotor gearbox vibration.

2. It can be seen from Table 4 that the overall amplitudes of the photocell averages are, in two out of three cases (hover and anti-clockwise tail rotor turn), greater than the AC generator averages. This provides a general indicator that the photocell is a more accurate phase reference in these flight conditions than the AC generator. The exception for the clockwise tail rotor turn data may be due to the relatively low levels of tail rotor torque in this flight condition.

3. With the exception of the clockwise tail rotor turn, the amplitudes of the gear mesh harmonics in the photocell averages are nearly all greater than those in the AC generator averages. This provides additional evidence that the photocell is a better phase reference than the AC generator in these flight conditions. The amplitude ratios for the gear mesh harmonics, plotted in Figure 38, show very little agreement

with the mathematical model however. As predicted, this is most probably due to the assumption in the model that the phase jitter is normally distributed.

Table 4. Synchronous Average Amplitudes

#	AC Generator Average (G_{RMS})	Photocell Average (G_{RMS})	Difference Average (G_{RMS})	Difference / AC Generator (%)
A	4.125	3.915	0.278	6.74
B	4.789	4.656	0.194	4.05
C	4.691	4.612	0.156	3.33
D	4.047	4.005	0.148	3.66
E	2.756	2.767	0.112	4.06
F	5.252	5.127	0.183	3.48
G	5.137	5.001	0.227	4.42
H	3.309	3.834	0.759	22.9
I	4.485	4.165	0.801	17.9
J	2.522	3.650	1.588	63.0

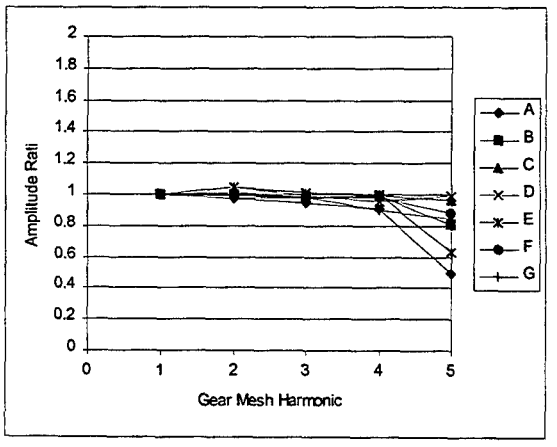

Figure 37. Amplitude Ratios of Gear Mesh Harmonics for Forward Flight (Photocell / AC Generator).

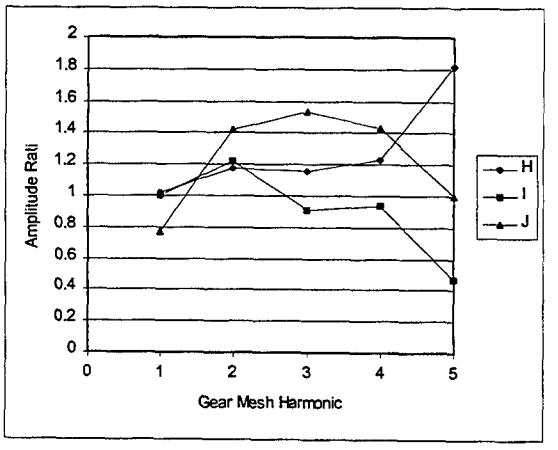

Figure 38. Amplitude Ratios of Gear Mesh Harmonics for Hover Flight (Photocell / AC Generator).

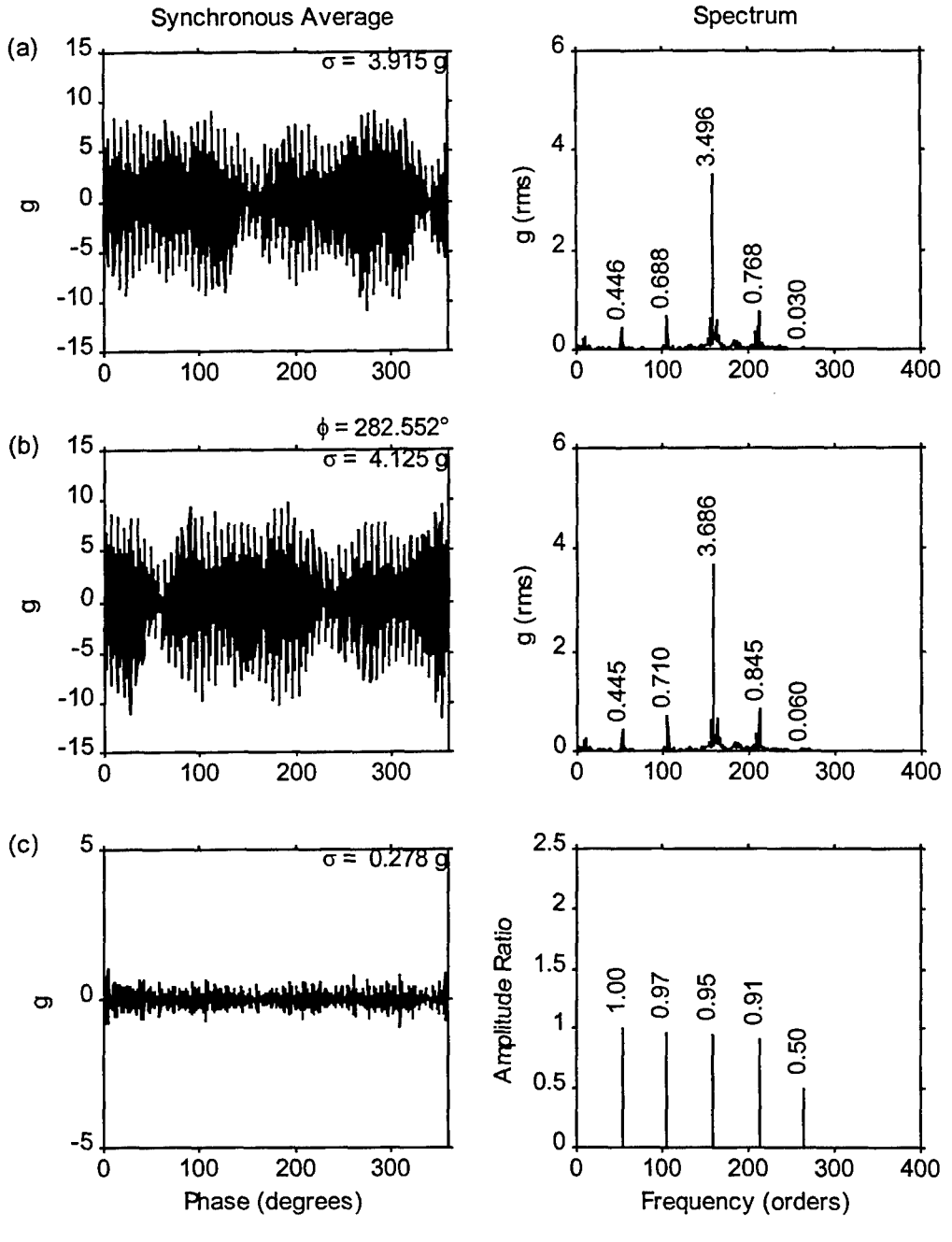

Figure 39. Synchronous Averages for Straight & Level Flight, 60% Torque

a) using the photocell signal,

b) using the AC generator signal (ϕ = phase offset of (b) to (a)),

c) difference between (a) and phase shifted (b), and amplitude ratios of gear mesh harmonics.

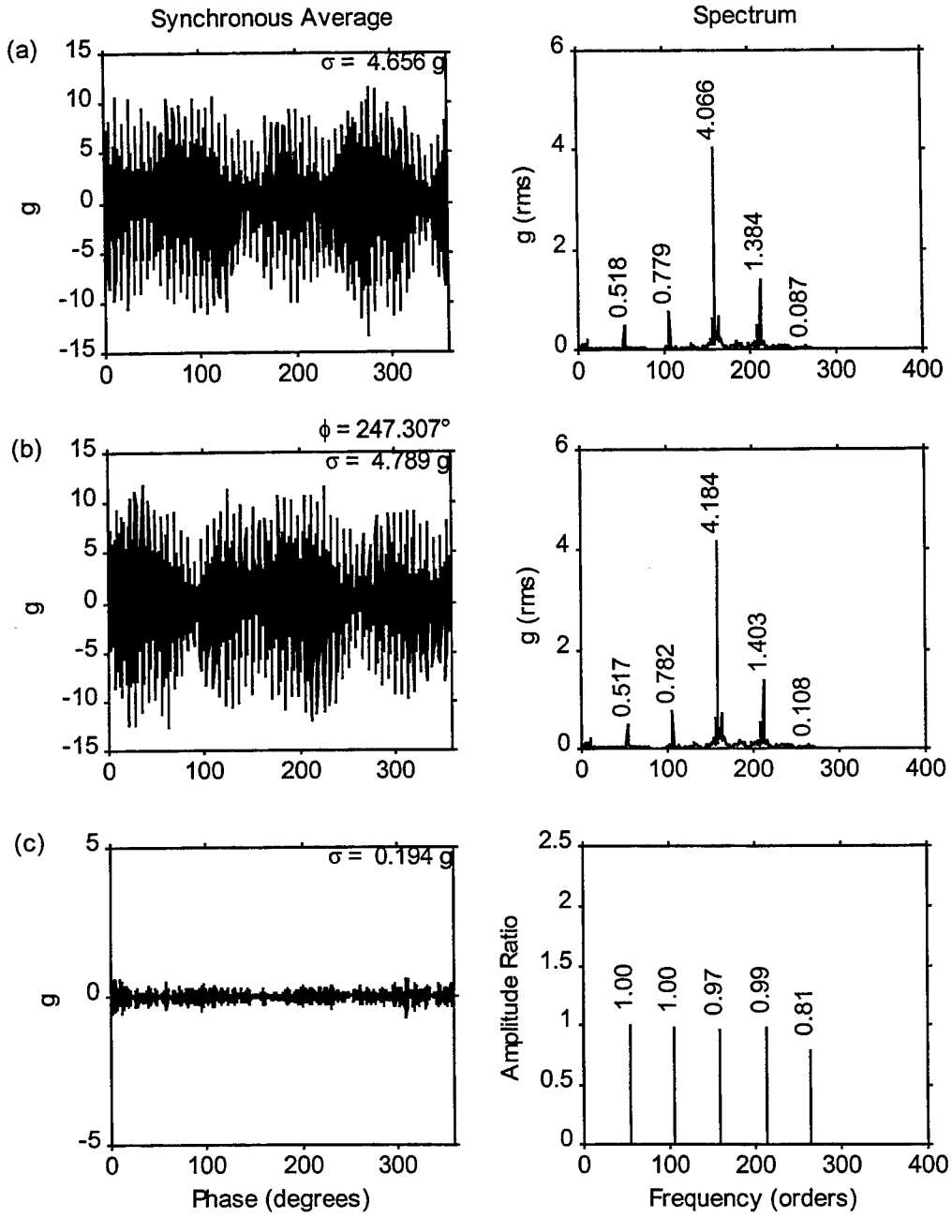

Figure 40. Synchronous Averages for Straight & Level Flight, 70% Torque

a) using the photocell signal,

b) using the AC generator signal (ϕ = phase offset of (b) to (a)),

c) difference between (a) and phase shifted (b), and amplitude ratios of gear mesh harmonics.

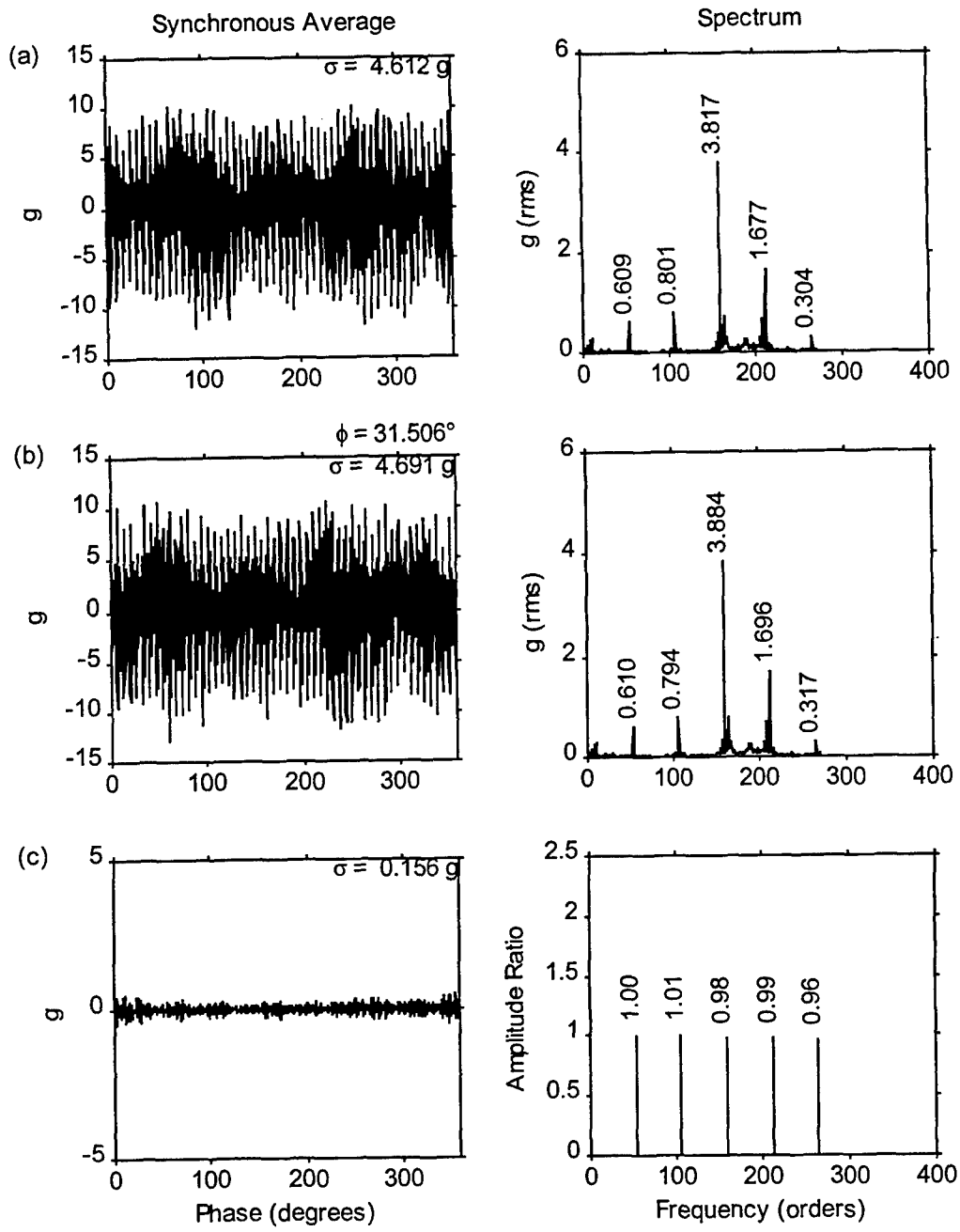

Figure 41. Synchronous Averages for Straight & Level Flight, 80% Torque

a) using the photocell signal,

b) using the AC generator signal (ϕ = phase offset of (b) to (a)),

c) difference between (a) and phase shifted (b), and amplitude ratios of gear mesh harmonics.

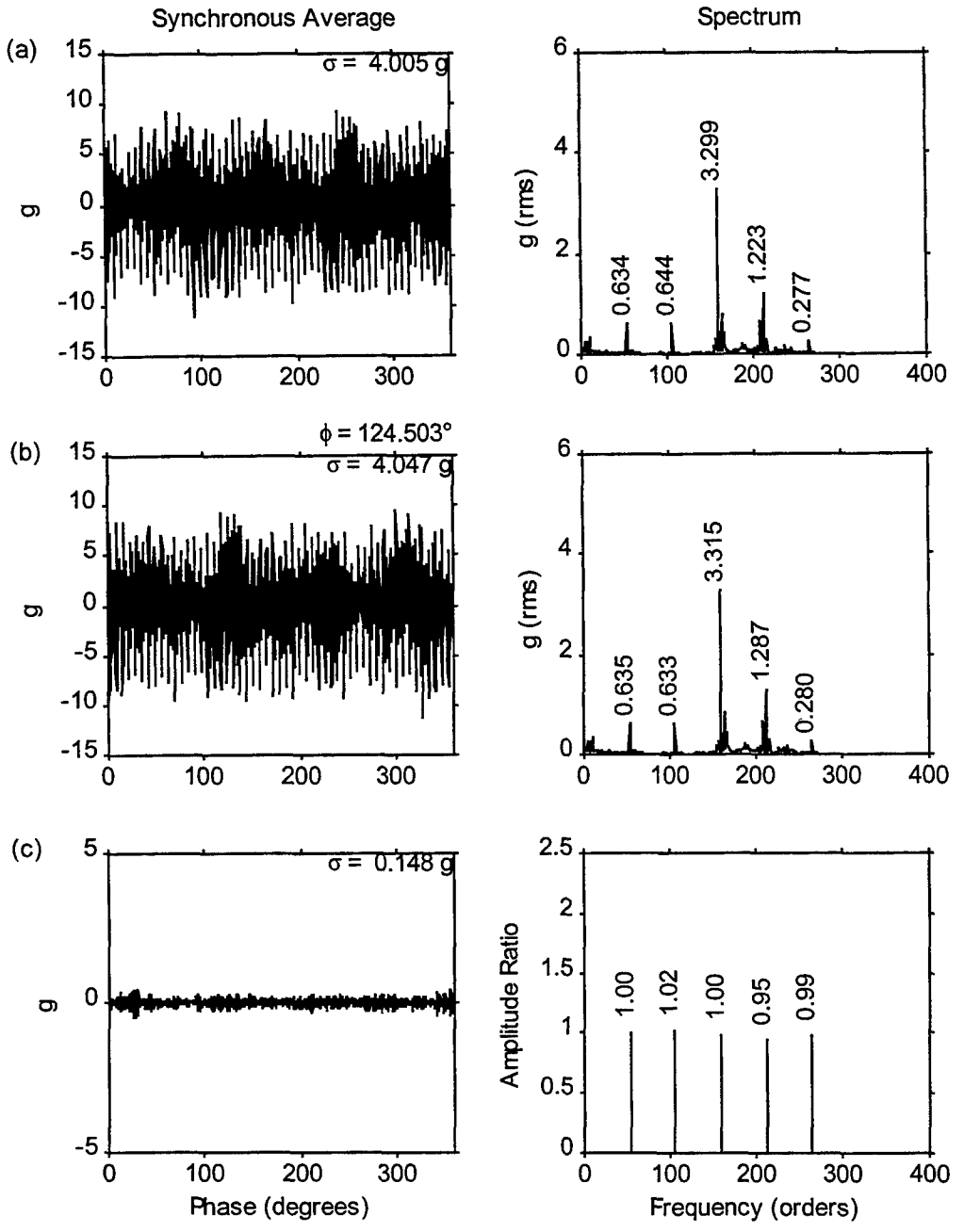

Figure 42. Synchronous Averages for Straight & Level Flight, 90% Torque

a) using the photocell signal,

b) using the AC generator signal (ϕ = phase offset of (b) to (a)),

c) difference between (a) and phase shifted (b), and amplitude ratios of gear mesh harmonics.

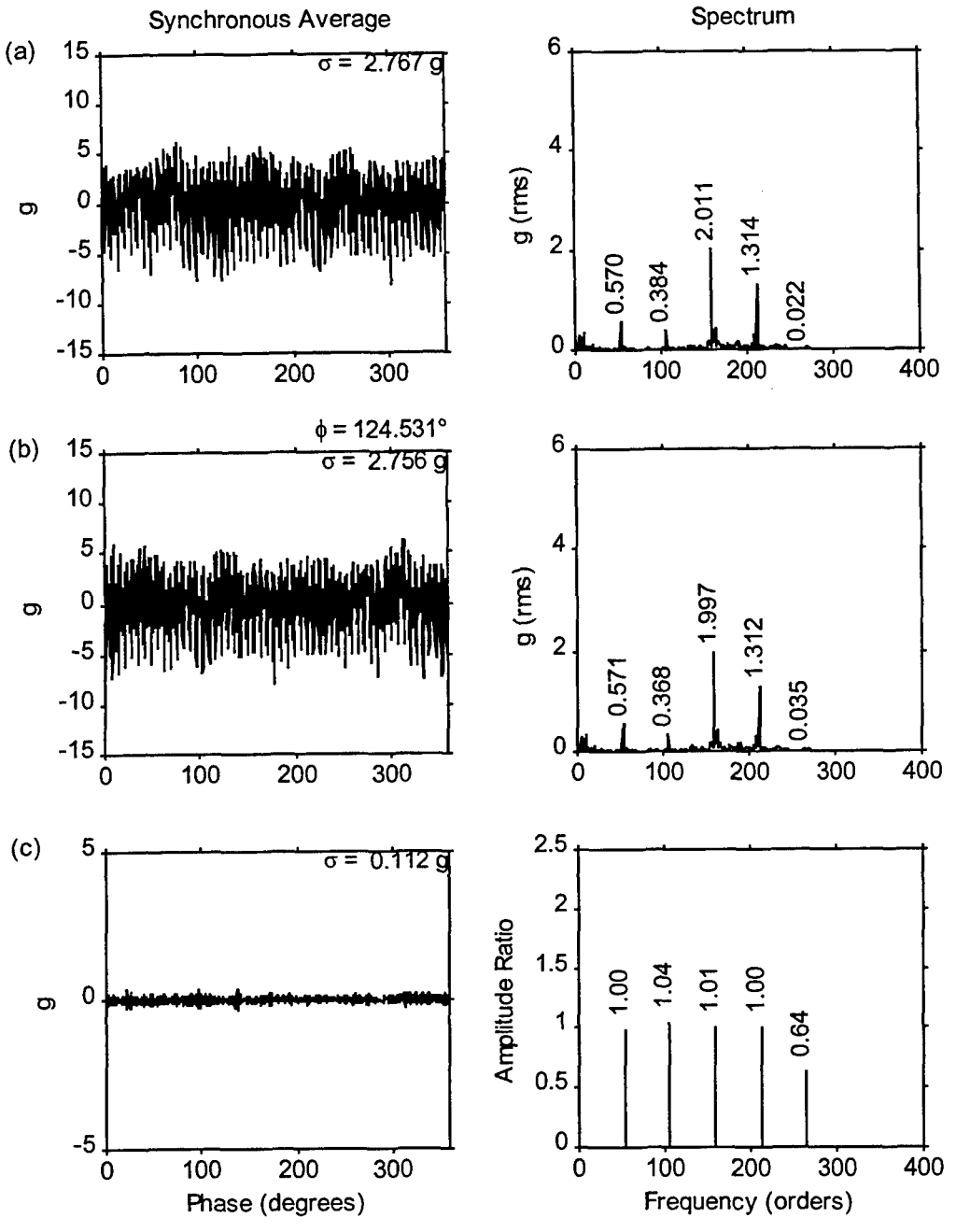

Figure 43. Synchronous Averages for Straight & Level Flight, 100% Torque

a) using the photocell signal,

b) using the AC generator signal (ϕ = phase offset of (b) to (a)),

c) difference between (a) and phase shifted (b), and amplitude ratios of gear mesh harmonics.

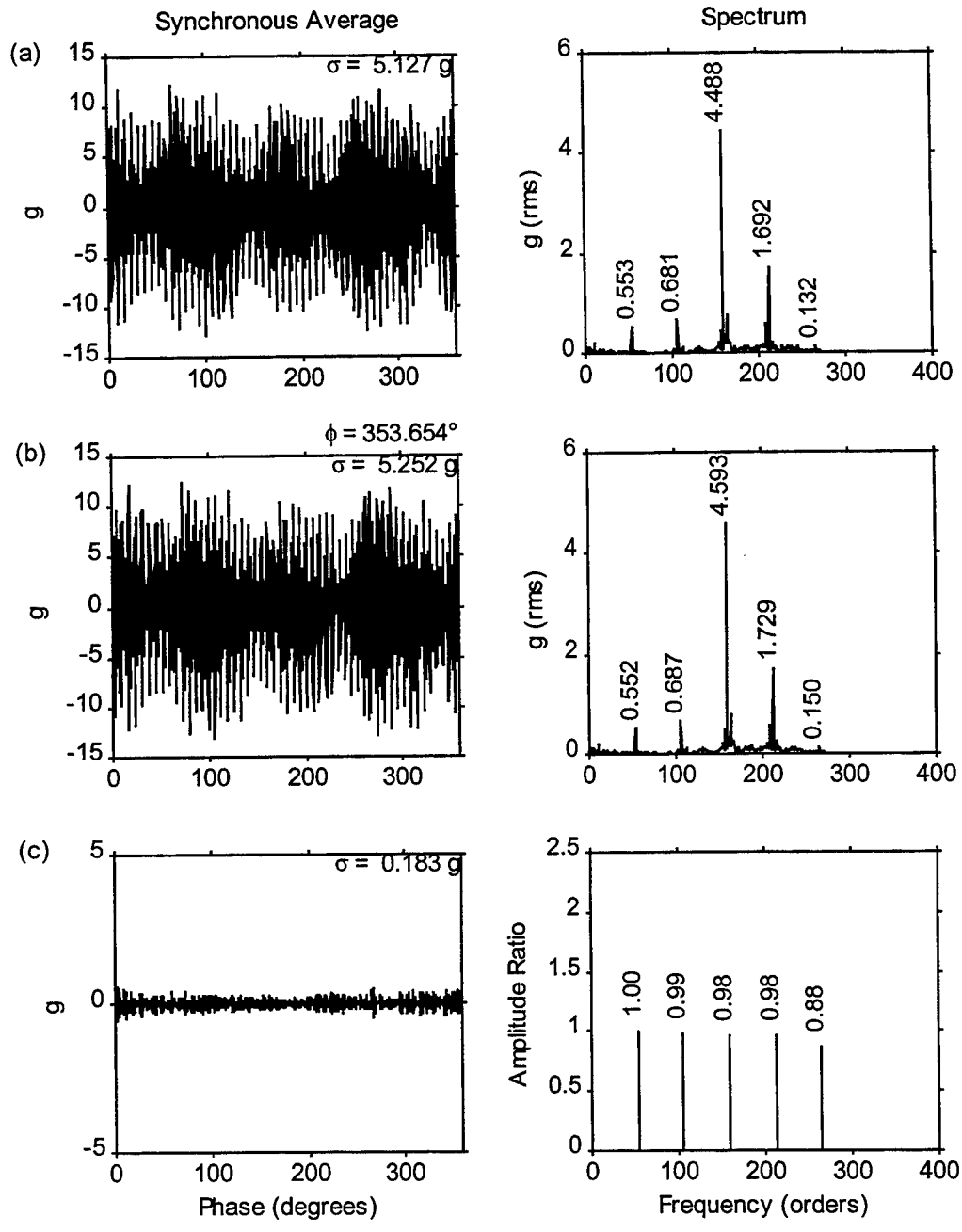

Figure 44. Synchronous Averages for Right Turn, 30° Bank

a) using the photocell signal,

b) using the AC generator signal (ϕ = phase offset of (b) to (a)),

c) difference between (a) and phase shifted (b), and amplitude ratios of gear mesh harmonics.

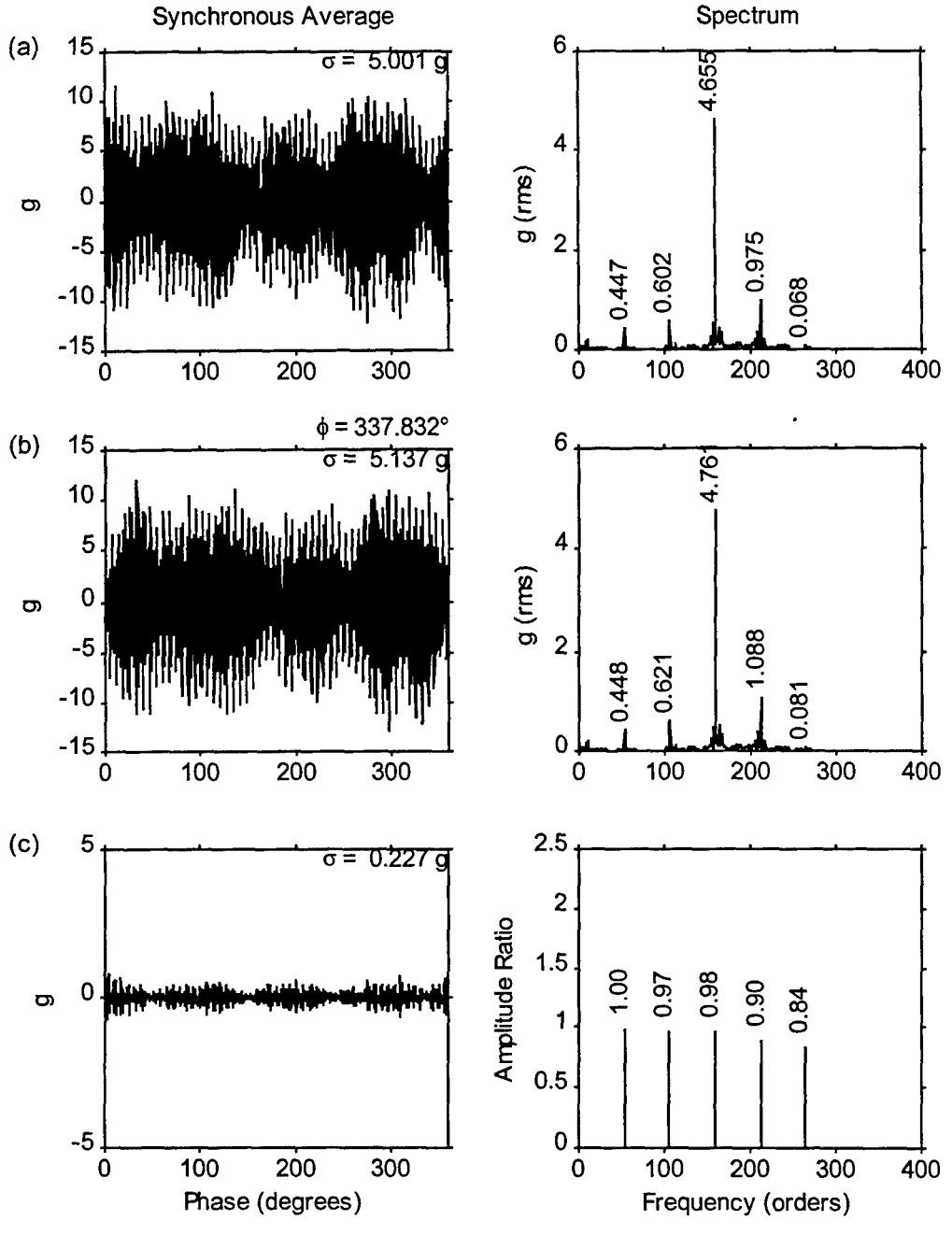

Figure 45. Synchronous Averages for Right Turn, 45° Bank

a) using the photocell signal,

b) using the AC generator signal (ϕ = phase offset of (b) to (a)),

c) difference between (a) and phase shifted (b), and amplitude ratios of gear mesh harmonics.

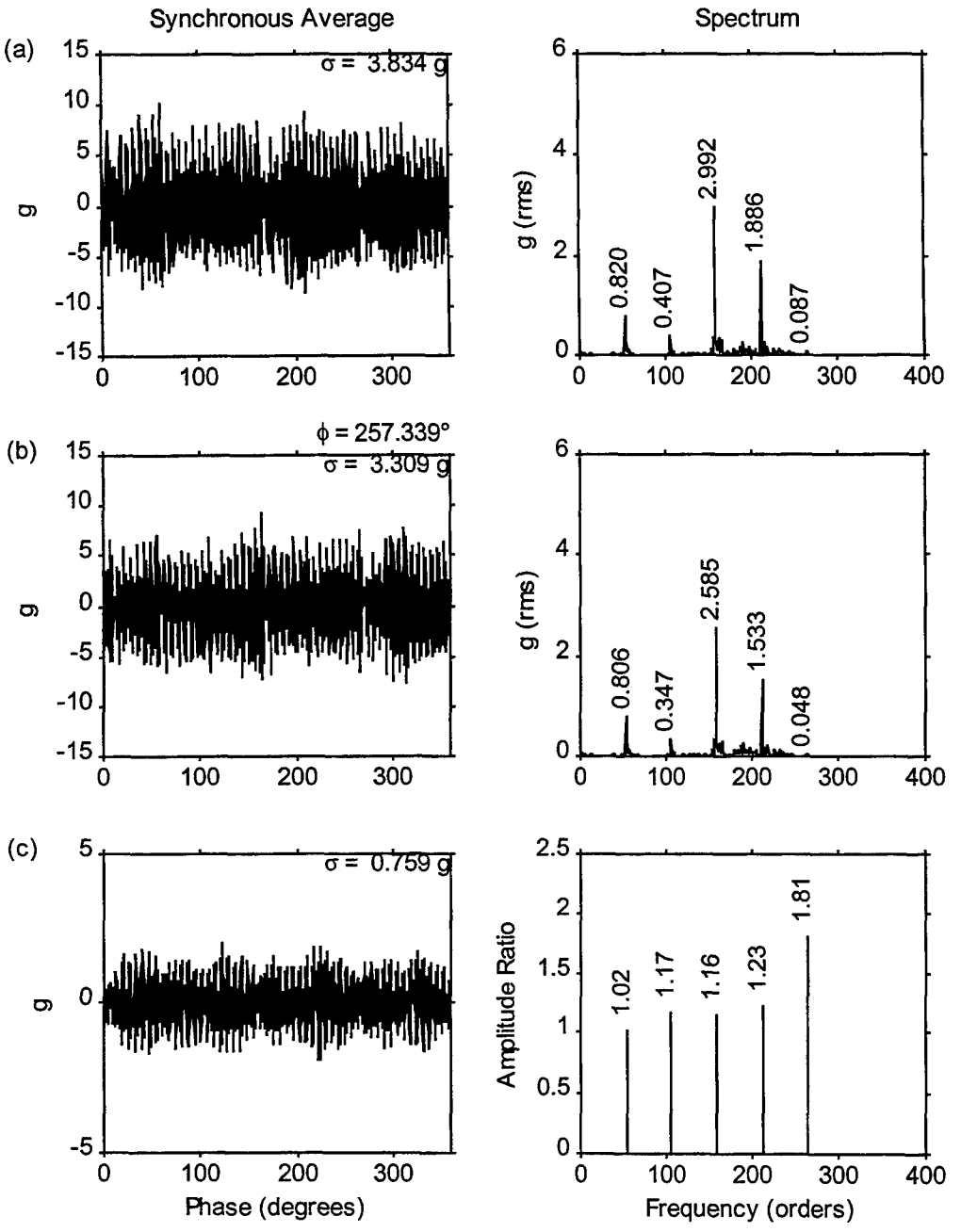

Figure 46. Synchronous Averages for Hover

a) using the photocell signal,

b) using the AC generator signal (ϕ = phase offset of (b) to (a)),

c) difference between (a) and phase shifted (b), and amplitude ratios of gear mesh harmonics.

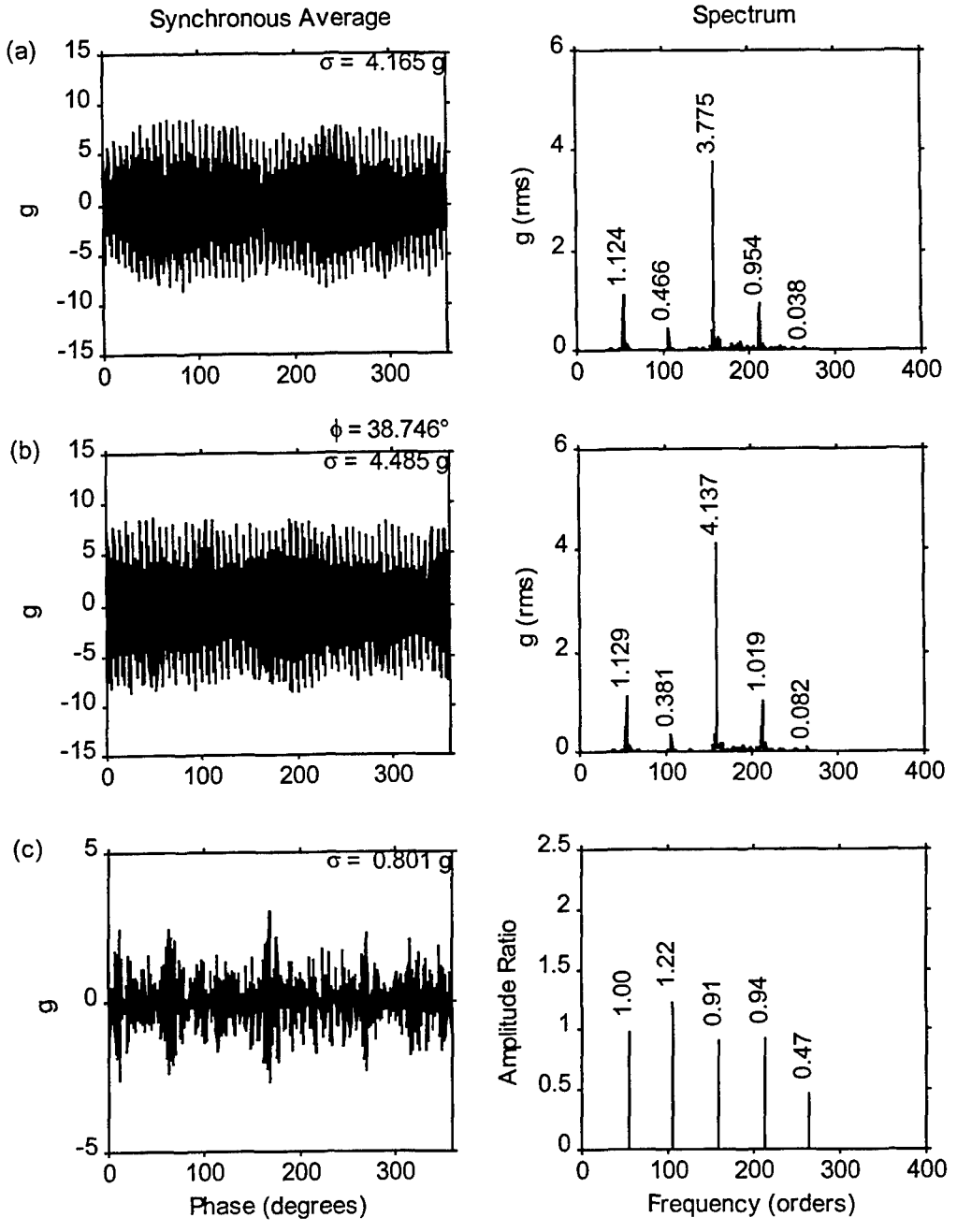

Figure 47. Synchronous Averages for Clockwise Tail Rotor Turn

a) using the photocell signal,

b) using the AC generator signal (ϕ = phase offset of (b) to (a)),

c) difference between (a) and phase shifted (b), and amplitude ratios of gear mesh harmonics.

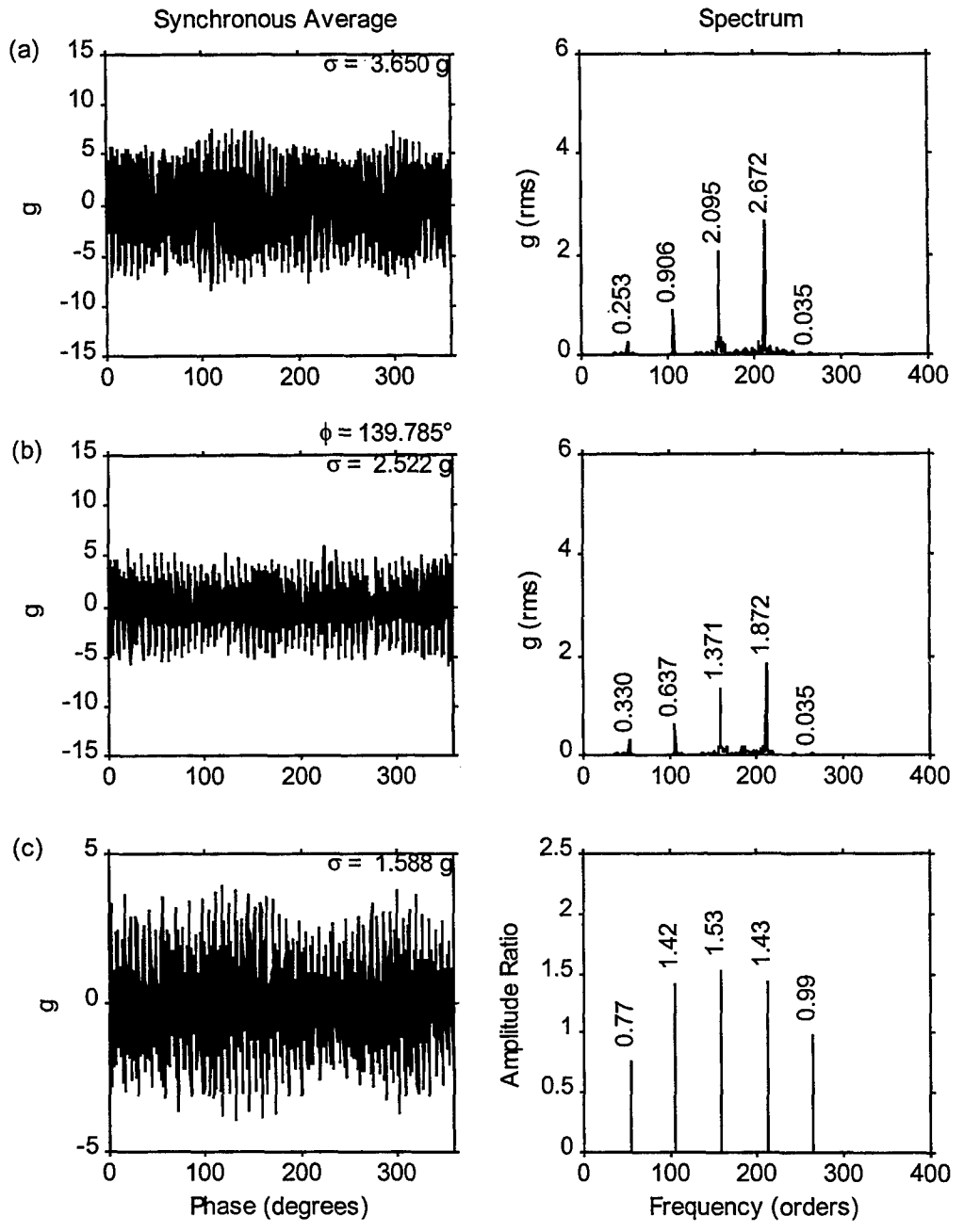

Figure 48. Synchronous Averages for Anti-Clockwise Tail rotor Turn

a) using the photocell signal,

b) using the AC generator signal (ϕ = phase offset of (b) to (a)),

c) difference between (a) and phase shifted (b), and amplitude ratios of gear mesh harmonics.

5.5 Measurement Errors

Errors in the measurement of the signal phase can be attributed to the causes listed below. It is not possible to accurately determine the overall measurement error, however, as this would require a measurement system that is more accurate than those used. Nevertheless, the trends identified in the phase difference distributions suggest that the measurement error must be small enough to produce the narrowest PDF (straight and level flight at 100% torque), which has a standard deviation of only 0.104°. Thus, the measurement error would be expected to be of a similar magnitude, or approximately 0.1°.

5.5.1 Zero-Crossing Error

As the positions of the zero-crossings are determined by linearly interpolating between adjacent samples above and below the zero-crossing threshold, there will inevitably be some difference between the interpolated zero-crossings and the true zero-crossings. This error will diminish as the sample rate increases.

Typical examples of the AC generator and photocell signals, are shown below (Figure 49 to Figure 52). In both cases, it can be seen that the sample rate is sufficiently high to reduce this error to a very low level, and that linear interpolation is not an unreasonable method of determining the positions of the zero-crossings. In either case, the maximum error will be limited to one sample period (71.25 μs), but should be considerably less than this. At an average tail rotor speed of 1190 rpm, one sample period corresponds to approximately 0.5°.

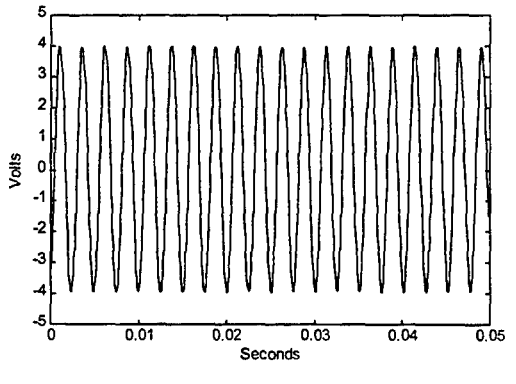

Figure 49. Typical AC Generator Signal.

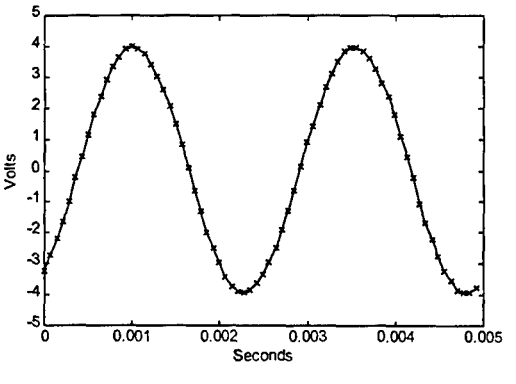

Figure 51. AC Generator Signal Detail.

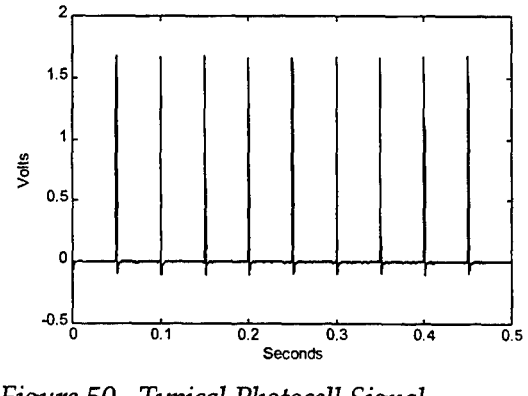

Figure 50. Typical Photocell Signal.

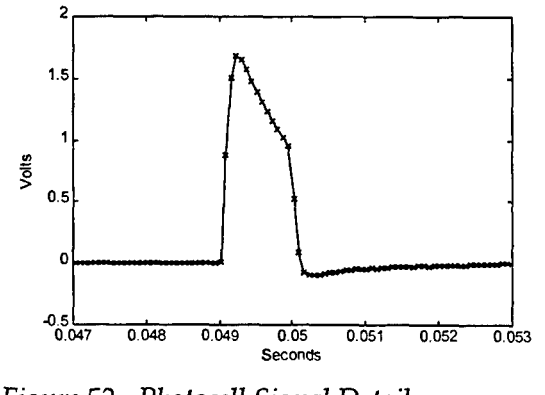

Figure 52. Photocell Signal Detail.

5.5.2 Phase Interpolation Error Between Zero-Crossings

As the phase of the tail rotor is linearly interpolated between the positive-going zero-crossings of the phase signals, there will inevitably be some difference between the interpolated phase and the true phase. That is, the true phase may behave in a non-linear way between the zero-crossings. This error will be smaller for the AC generator signal, as it has approximately 19.85 zero-crossings for every one of the photocell signal. The error for the photocell could possibly be reduced, by placing reflective tape on the other tail rotor blades to give more pulses per revolution. However, this would require an evaluation of the lead/lag error between the blades.

Unfortunately, it is not possible to estimate this error without a phase reference signal that is more accurate than those available (eg from a shaft encoder). The substantial inertia of the tail rotor, however, will act to limit the rate of change of phase, and in the absence of large impulsive torques, the magnitude of this error would be expected to be similar to the zero-crossing error.

5.5.3 Other Errors

The following errors will all contribute to the overall measurement error, but were considered to be less significant than those above.

1. Photocell Triggering: The exact point at which the photocell is triggered by the reflective tape (ie how far the reflective tape penetrates the beam before triggering the photocell) may vary slightly from one revolution of the tail rotor to the next. This will be compounded to some extent by flapping of the rotor blade under the control inputs and dynamic loads experienced in flight.

2. Signal Noise/Interference: Noise or interference has the potential to make the signal zero-crossings appear earlier or later than their true positions. Noise introduced through tape recording and filtering processes has been found to be significant in previous investigations [4], but has been kept to a minimum here through the direct digital acquisition of data using the computer. Interference by the tail pylon strobes was observed in the photocell signal, but these strobes were turned off during the acquisition of all data.

3. Analogue-to-Digital Converter (ADC) Error: ADC errors will also make the signal zero-crossings appear earlier or later than their true positions. A 12-bit ADC will have at least ±½ bit of uncertainty in the measurement. With an input range of ±5 V, this corresponds to an uncertainty of approximately 1 mV.

4. AC Signal Distortion: The AC generator supplies power to a number of devices in the aircraft all of which have the potential to disturb or distort the signal waveform. Localised disturbances that cause the zero-crossing to move relative to its undisturbed position will affect the results. Continuous distortion of the waveform, however, should not affect the results, as the zero-crossing error will be constant.

6. Conclusions

This report has examined the relative jitter, due to dynamic tail drive shaft twist, between phase reference signals obtained from the main and tail rotor gearboxes in a S-70A-9 Black Hawk helicopter. The results from this, and a comparison of the synchronous averages of the tail rotor gearbox output shaft computed using these signals, has revealed the following:

1. There is significant evidence of dynamic twisting of the tail drive shaft during hover and tail rotor turns. This is most probably caused by tail rotor torque variations induced by pilot control pedal movements.

2. The level of this twisting is significant enough to affect the synchronous averaging of tail rotor gearbox vibration when using a phase reference signal derived from the main rotor gearbox.

3. During forward flight, the level of twisting is minimised, and both phase reference signals perform similarly well for synchronous averaging purposes. However, in the S-70A-9, it was discovered that undesirable vibration impulses were induced in the tail rotor gearbox vibration during these flight conditions. It was speculated that these impulses were caused by the aerodynamic interaction of the main rotor tip vortices on the tail rotor blades.

4. The (relatively simple) mathematical model developed to examine the theoretical effect of phase reference jitter on synchronous averaging proved to be difficult to apply to the data because of the lack of an absolute phase reference, and assumptions made in the model. Some qualitative agreement with the model was observed for the forward flight data, but no agreement was observed for the hover flight data.

From these results, the following recommendations are made:

1. Wherever possible, a tail rotor phase reference signal should be used in preference to a main rotor phase reference signal when synchronously averaging tail rotor gearbox vibration.

2. In the S-70 series of helicopters, tail rotor gearbox vibration should only be examined during hover, or very low forward speeds, to eliminate the potential for any undesirable vibration impulses to mask faults within the gearbox.

Acknowledgments

The author wishes to acknowledge Mr Brian Rebbechi for his suggestion to examine this aspect of helicopter gearbox vibration analysis, and Dr B. David Forrester and Dr Albert K. Wong for their advice.

References

1 Blunt, D.M., and Dutton, S.A., "A Lightweight Vibration Monitoring System for the S-70A-9 Black Hawk Transmission," DSTO Technical Report 0336, AR-009-697, November 1996.

2 Forrester, B.D., "Advanced Vibration Analysis Techniques for Fault Detection and Diagnosis in Geared Transmission Systems," PhD Thesis, Swinburne University of Technology, 1996.

3 Bowker, A.H., and Lieberman, G.J., "Engineering Statistics," 2nd Edition, Prentice-Hall Inc., 1972.

4 Blunt, D.M., "Variations in the AC Generator Period of a Sea King Helicopter," DSTO General Document 0004, AR-008-545, June 1994.

Appendix 1:
S-70A-9 Black Hawk Transmission

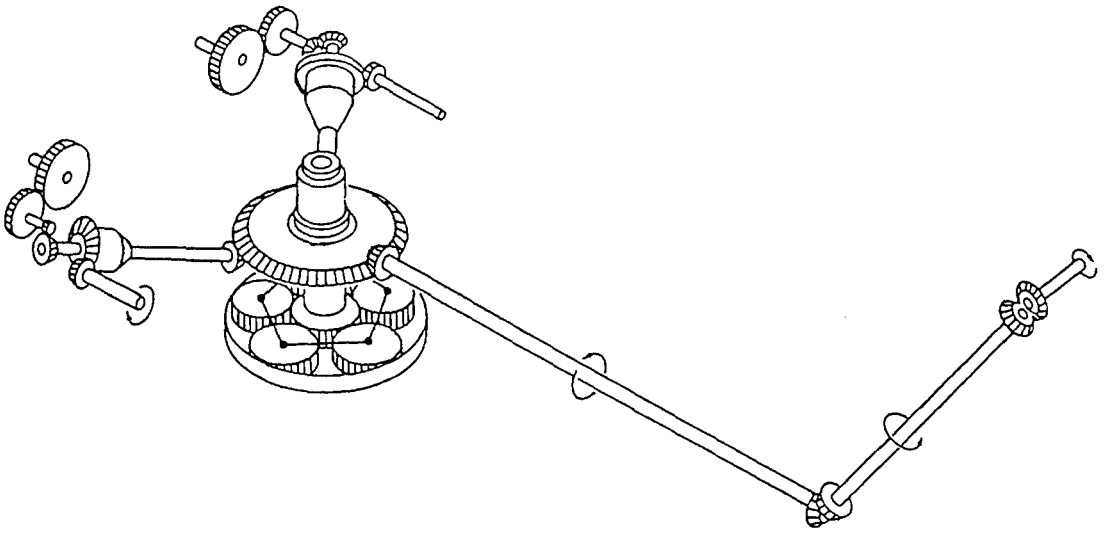

Shaft	RPM	Gear	Teeth	Mesh Freq (Hz)
Input Module				
High Speed Input Shaft	20900	Input Pinion	22	7663
Input Gear (Quill) Shaft	5748	Input Gear	80	7663
		Accessory Drive Take-off	76	7281
Accessory Drive Shaft	11806	Accessory Drive Gear	37	7281
Accessory Module				
Generator Drive Shaft	11806	Hydraulic Drive Take-off	56	11019
Hydraulic Drive Shaft	7186	Hydraulic Drive Gear	92	11019
Main Module				
Combining Pinion (Quill) Shaft	5748	Combining Pinion	21	2012
Crownwheel Shaft	1207	Lower Crownwheel Gear	100	2012
		Upper Crownwheel Gear	75	1509
		Sun Gear	62	980
Planet Gear (wrt Carrier)	708	Planet Gear	83	980
Ring Gear	0	Ring Gear	228	980
Tail Drive Shaft	4115	Tail Take-off Gear	22	1509
Planet Carrier/ Main Rotor	258	Lube Pump Take-off Gear	152	654
Lube Pump Drive Shaft	3268	Lube Pump Drive Gear	12	654
Intermediate Gearbox				
Input	4115	Input Pinion	25	1714
Output	3318	Output Gear	31	1714
Tail Rotor Gearbox				
Input	3318	Input Pinion	19	1051
Output	1190	Output Gear	53	1051

Appendix 2: MATLAB M Files

ATTEN.M

```
function atten(bw,sigma,conf,n)
%atten(bw,sigma,conf,n)
%Plots the amplitude response of a signal average with tacho jitter.
%bw = upper frequency limit (shaft orders)
%sigma = max standard deviation of jitter (degrees)
%conf = confidence level [0,1)
%n = number of averages
%DMB 29/10/97
freq=(0:bw);
s=(0:0.1:sigma)*pi/180;
conlim=mychi2conf(conf,n);
clf;
set(gca,'colororder',[0 0 0]);
set(gca,'linestyleorder','-|--|-.|:');
set(gca,'box','on');
set(gca,'ylim',[0 1.05]);
for i=1:length(s),
   t=-0.5*s(i)^2*freq.^2;
   a(i,:)=exp(t);
   b(i,:)=exp(conlim(1)^2*t); %LCL
   c(i,:)=exp(conlim(2)^2*t); %UCL
   ll(i,:)=sprintf('\\sigma = %1.1f\\circ',s(i)*180/pi);
   hp(i)=patch([freq     fliplr(freq)],[b(i,:),fliplr(c(i,:))],[0.85     0.85
0.85]);
end
hold on
h=plot(freq,a);
hold off
xlabel('Frequency (shaft orders)');
ylabel('Amplitude');
title(sprintf('Amplitude Response (%i%% Conf., N = %i)',conf*100,n));
legend(h,ll,3);
```

SPEED.M

```
function speed(tail,main,t1,t2,y1,y2);
% Calculate and plot tacho speed variations
fs=4000000/95; %total sample rate
fs=fs/3; %sample rate per channel
time = (0:length(tail)-1)'/fs; %create time vector
main = main * 1107225/21976768; % convert to tail rotor angle
p=polyfit(time,tail,1); %linear regression of tail tacho
y=polyval(p,time); %evaluate linear fit
vt = (tail - y)*360; % subtract linear fit and convert to degrees
vm = (main -y)*360; % subtract linear fit and convert to degrees
vt = decimate(vt-mean(vt),100); %subtract mean and decimate
vm = decimate(vm-mean(vm),100); %subtract mean and decimate
time = (0:length(vt)-1)'*100/fs;
figure(gcf);clf;
set(gcf,'defaultaxesfontsize',8);
set(gcf,'defaulttextfontsize',8);
set(gcf,'defaultaxestickdirmode','manual');
set(gcf,'defaultaxestickdir','out');
set(gcf,'defaultaxesbox','on');
set(gcf,'position',[100,350,680,350]);
subplot(1,2,1);
h1=plot(time,vt,'k-',time,vm,'k--');
set(gca,'XLim',[0 max(time)])
set(gca,'YLim',[-60 60])
```

```
xlabel('Time (s)');
ylabel('Angle (deg)');
title('Lead/Lag of Tail Rotor Angle');
legend(h1,'Photocell','Generator',0);
x1 = round(length(vt)*t1/max(time));
x2 = round(length(vt)*t2/max(time));
subplot(1,2,2);
h2=plot(time(x1:x2),vt(x1:x2),'k-',time(x1:x2),vm(x1:x2),'k--');
set(gca,'XLim',[time(x1) time(x2)])
set(gca,'YLim',[y1 y2])
title('Lead/Lag of Tail Rotor Phase Angle');
xlabel('Time (s)');
ylabel('Angle (deg)');
legend(h2,'Photocell','Generator',0);
```

DPHASE.M

```
function delta = dphase(main,tail);
main = main * 1107225/21976768;
delta = (tail-main)*360;
delta = delta - mean(delta);
```

PLOTD.M

```
function plotd(data,r);
d=decimate(data,r);
time = (0:length(d)-1).'*r*95*3/4E6;
plot(time,d,'k-');
set(gca,'ylim',[-1.2,1.2]);
set(gca,'xlim',[0,time(length(time))]);
xlabel('Time (s)');
ylabel('Angle (deg)');
title('Phase Difference');
```

PDF.M

```
function pdf(delta,xmin,xmax,ymax,nbins);
% pdf(delta,xmin,xmax,ymax,nbins)
% Compute probability density function from xmin to xmax using nbins.
mu = mean(delta);
sigma = std(delta);
% specify mid points of bins for hist function
dx = (xmax-xmin)/nbins;
x = ((0:nbins-1)+0.5)*dx + xmin;
% compute and plot histogram
n = hist(delta,x);
p = n/sum(n)/dx;
hs = stairs(x-0.5*dx,p,'k-');
set(hs,'linewidth',1);
haxes = gca;
set(haxes,'XLim',[xmin xmax])
set(haxes,'YLim',[0 ymax])
% Label graph
set(gcf,'position',[10 320 500 400])
title('PDF of Phase Difference');
xlabel('Angle (deg)');
ylabel('Probability Density');
% Print standard deviation
xtxt = xmin + 0.95*(xmax-xmin);
ytxt = 0.9 * ymax;
str = sprintf('\\sigma = %6.3f\\circ',sigma);
hsigma = text(xtxt,ytxt,str);
set(hsigma,'VerticalAlignment','Top');
set(hsigma,'HorizontalAlignment','right');
% Print max deviation
str = sprintf('max = %6.3f\\circ',max(delta));
ytxt = 0.8 * ymax;
```

```
hmu = text(xtxt,ytxt,str);
set(hmu,'VerticalAlignment','Bottom');
set(hmu,'HorizontalAlignment','right');
% Print min deviation
str = sprintf('min = %6.3f\\circ',min(delta));
hsigma = text(xtxt,ytxt,str);
set(hsigma,'VerticalAlignment','Top');
set(hsigma,'HorizontalAlignment','right');
% compute and plot normal distribution
xx = xmin + (0:266)/266*(xmax-xmin);
pn = 1/sigma/sqrt(2*pi)*exp(-xx.^2/2/sigma.^2);
hold on;
hpn = plot(xx,pn,'k:');
set(hpn,'linewidth',0.5);
legend(hpn,'Normal Distribution',2)
hold off;
```

PSHIFT.M

```
function y = pshift (x, p);
% y = pshift (x, p)
% y = x shifted to the right by p points via fft(x)
% x = signal
% p = number of points to shift
fx = fftshift(fft(x));
fz = exp(-j*2*pi*(-length(x)/2:length(x)/2-1)*p/length(x));
fy = fftshift(fx .* fz);
y = ifft(fy);
```

XCORR.M

```
function z = xcorr(s1,s2)
% z = xcorr(s1,s2)
% z = circular cross correlation of s1 and s2 computed via fft
% s1 = signal 1
% s2 = signal 2 (must be the same length as s1)
f1 = fft(s1);
f2 = fft(s2);
xspec = f1 .* conj(f2);
z = ifft(xspec);
```

PSYNC1.M

```
function xcmax = psync1(phi,s1,s2)
% xcmax = psync1(phi)
% xcmax = max cross correlation of signals s1 and s2
% phi = number of points to shift s2 to the right
% s1 = signal 1
% s2 = signal 2
% index = point of max correlation
global index
[xcmax,index] = max(real(xcorr(s1,real(pshift(s2,phi)))));
xcmax = -xcmax;
```

COMPSIG2.M

```
function [phi,ds]=compsig2(s1,s2);
% [phi,ds]=compsig(s1,s2)
% Compares s1 to s2 by finding the phase difference and removing it from s2.
% Plots signal and power spectra of s1, s2, and the difference signal.
% phi = number of points that s2 lags s1
% ds = difference signal
% s1 = signal 1
% s2 = signal 2 (must be same length as s1)
% index = point of max correlation computed by 'psync1'
% DMB 27/10/97
global index
% use fmin to find the phase shift that produces the max correlation
phi = fmin('psync1',0,length(s2)-1,foptions,s1,s2);
```

```
phi = mod(phi + index - 1,length(s2));
% compute difference signal
ds = s1 - real(pshift(s2,phi));

% plot s1
figure(gcf);clf;
set(gcf,'position',[50,60,480,600]);
set(gcf,'defaultaxesfontsize',8);
set(gcf,'defaulttextfontsize',8);
set(gcf,'defaultaxestickdirmode','manual');
set(gcf,'defaultaxestickdir','out');
set(gcf,'defaultaxesbox','on');
x = 360*(0:length(s1)-1)/length(s1);
f = (0:length(s1)/2-1);
subplot(3,2,1),plot(x,s1,'k');
set(gca,'xlim',[0,360]),set(gca,'ylim',[-15,15]);
title('Synchronous Average'),ylabel('g'),text(-100,15,'(a)');
str = sprintf('\\sigma = %6.3f g',std(s1));
ht = text(360,15,str);
set(ht,'VerticalAlignment','Top');
set(ht,'HorizontalAlignment','Right');
fs1 = fft(s1);
subplot(3,2,2);
plot(f(1:400),abs(fs1(1:400))*sqrt(2)/length(fs1),'k');
set(gca,'xlim',[0,400]),set(gca,'ylim',[0,6]);
%plot(f,abs(fs(1:length(fs)/2))*sqrt(2)/length(fs),'k');
%set(gca,'xlim',[0,length(fs)/2-1]),set(gca,'ylim',[0,6]);
title('Spectrum'),ylabel('g (rms)');
for i=1:5,
   str = sprintf('%6.3f',abs(fs1(i*53+1))*sqrt(2)/length(fs1));
   ht = text(f(i*53+1),abs(fs1(i*53+1))*sqrt(2)/length(fs1),str);
   set(ht,'VerticalAlignment','Middle');
   set(ht,'HorizontalAlignment','Left');
   set(ht,'Rotation',90);
end

% plot s2
subplot(3,2,3),plot(x,s2,'k');
set(gca,'xlim',[0,360]),set(gca,'ylim',[-15,15]);
ylabel('g'),text(-100,15,'(b)');
str = sprintf('\\sigma = %6.3f g',std(s2));
ht = text(360,15,str);
set(ht,'VerticalAlignment','Top');
set(ht,'HorizontalAlignment','Right');
str = sprintf('\\phi = %6.3f\\circ',phi*360/length(s2));
ht = text(360,15,str);
set(ht,'VerticalAlignment','Bottom');
set(ht,'HorizontalAlignment','Right');
fs2 = fft(s2);
subplot(3,2,4);
plot(f(1:400),abs(fs2(1:400))*sqrt(2)/length(fs2),'k');
set(gca,'xlim',[0,400]),set(gca,'ylim',[0,6]);
%plot(f,abs(fs(1:length(fs)/2))*sqrt(2)/length(fs),'k');
%set(gca,'xlim',[0,length(fs)/2-1]),set(gca,'ylim',[0,6]);
ylabel('g (rms)');
for i=1:5,
   str = sprintf('%6.3f',abs(fs2(i*53+1))*sqrt(2)/length(fs2));
   ht = text(f(i*53+1),abs(fs2(i*53+1))*sqrt(2)/length(fs2),str);
   set(ht,'VerticalAlignment','Middle');
   set(ht,'HorizontalAlignment','Left');
   set(ht,'Rotation',90);
end

% plot difference signal
subplot(3,2,5),plot(x,ds,'k');
set(gca,'xlim',[0,360]),set(gca,'ylim',[-5,5]);
xlabel('Phase (degrees)'),ylabel('g'),text(-100,5,'(c)');
str = sprintf('\\sigma = %6.3f g',std(ds));
```

```
ht = text(360,5,str);
set(ht,'VerticalAlignment','Top');
set(ht,'HorizontalAlignment','Right');
fs = fft(ds);
subplot(3,2,6);
%plot(f(1:400),abs(fs1(1:400))./abs(fs2(1:400)),'k');
set(gca,'xlim',[0,400]),set(gca,'ylim',[0,2.5]);
%plot(f,abs(fs(1:length(fs)/2))*sqrt(2)/length(fs),'k');
%set(gca,'xlim',[0,length(fs)/2-1]),set(gca,'ylim',[0,1.2]);
xlabel('Frequency (orders)'),ylabel('Amplitude Ratio');
for i=1:5,
   hl=line([f(i*53+1),f(i*53+1)],[0,abs(fs1(i*53+1))/abs(fs2(i*53+1))]);
   set(hl,'color',[0,0,0]);
   str = sprintf('%6.2f',abs(fs1(i*53+1))/abs(fs2(i*53+1)));
   ht = text(f(i*53+1),abs(fs1(i*53+1))/abs(fs2(i*53+1)),str);
   set(ht,'VerticalAlignment','Middle');
   set(ht,'HorizontalAlignment','Left');
   set(ht,'Rotation',90);
end
```

DISTRIBUTION LIST

Synchronous Averaging of Helicopter Tail Rotor Gearbox Vibration:
Phase Reference Considerations

D.M. Blunt

AUSTRALIA

DEFENCE ORGANISATION

Task Sponsor **DGTA**

S&T Program

Chief Defence Scientist
FAS Science Policy } shared copy
AS Science Corporate Management
Director General Science Policy Development
Counsellor Defence Science, London (Doc Data Sheet)
Counsellor Defence Science, Washington (Doc Data Sheet)
Scientific Adviser to MRDC Thailand (Doc Data Sheet)
Director General Scientific Advisers and Trials/Scientific Adviser Policy and Command (shared copy)
Navy Scientific Adviser
Scientific Adviser - Army (Doc Data Sheet and distribution list only)
Air Force Scientific Adviser
Director Trials

Aeronautical and Maritime Research Laboratory

Director
Chief of Airframes and Engines Division
Research Leader Propulsion
A.K. Wong
B. Rebbechi
B.D. Forrester
D.M. Blunt (5 copies)
M.A. Shilo
P. Marsden
W. Wang

DSTO Library

Library Fishermens Bend
Library Maribyrnong
Library Salisbury (2 copies)
Australian Archives
Library, MOD, Pyrmont (Doc Data sheet only)

Capability Development Division

Director General Maritime Development
Director General Land Development (Doc Data Sheet only)
Director General C3I Development (Doc Data Sheet only)

Navy

SO (Science), Director of Naval Warfare, Maritime Headquarters Annex, Garden Island, NSW 2000. (Doc Data Sheet only)

S-70B APLOGMAN, Naval Aviation Logistics Management Squadron, Naval Support Command, Locked Bag 12, Pyrmont NSW 2009.

Army

ABCA Office, G-1-34, Russell Offices, Canberra (4 copies)

SO (Science), DJFHQ(L), MILPO Enoggera, Queensland 4051 (Doc Data Sheet only)

NAPOC QWG Engineer NBCD c/- DENGRS-A, HQ Engineer Centre Liverpool Military Area, NSW 2174 (Doc Data Sheet only)

A25 Logistics Engineer, Army Aircraft Logistics Management Squadron, Army Airfield, Oakey QLD 4401

Air Force

DTA, Headquarters Logistics Command

Tech Reports, CO Engineering Squadron, Aircraft Research and Development Unit, RAAF Base Edinburgh SA 5111

Intelligence Program

DGSTA Defence Intelligence Organisation

Corporate Support Program (libraries)

OIC TRS, Defence Regional Library, Canberra

Officer in Charge, Document Exchange Centre (DEC) (Doc Data Sheet and distribution list only)

*US Defence Technical Information Center, 2 copies

*UK Defence Research Information Centre, 2 copies

*Canada Defence Scientific Information Service, 1 copy

*NZ Defence Information Centre, 1 copy

National Library of Australia, 1 copy

UNIVERSITIES AND COLLEGES

Australian Defence Force Academy
Library
Head of Aerospace and Mechanical Engineering

Deakin University, Serials Section (M list), Deakin University Library, Geelong VIC 3217

Senior Librarian, Hargrave Library, Monash University

Librarian, Flinders University

Dr I.M. Howard, Department of Mechanical Engineering, Curtin University of Technology, GPO Box U1987 Perth WA 6001

Associate Professor R.B. Randall, School of Mechanical and Manufacturing Engineering, University of New South Wales, Sydney NSW 2052

Dr Y. Gao, School of Mechanical and Manufacturing Engineering, University of New South Wales, Sydney NSW 2052

Professor J. Mathew, Centre for Machine Condition Monitoring, Monash University

OTHER ORGANISATIONS

NASA (Canberra)

AGPS

OUTSIDE AUSTRALIA

ABSTRACTING AND INFORMATION ORGANISATIONS

INSPEC: Acquisitions Section Institution of Electrical Engineers
Library, Chemical Abstracts Reference Service
Engineering Societies Library, US
Materials Information, Cambridge Scientific Abstracts, US
Documents Librarian, The Center for Research Libraries, US

INFORMATION EXCHANGE AGREEMENT PARTNERS

Acquisitions Unit, Science Reference and Information Service, UK
Library - Exchange Desk, National Institute of Standards and Technology, US

US NAVY

Mr Bill Hardman, Naval Air Warfare Center Aircraft Division, Building 106 AIR442, 22195 Elmer Road Unit 4, Patuxent River MD 20670-1534, USA. (2 copies)

UK MINISTRY OF DEFENCE

Cdr Trevor Pritchard, MOD(PE) DHO.H/POL, Ministry of Defence (PE) Abbey Wood Walnut 10#70, Bristol BS34 8JH, UK.

OTHER ORGANISATIONS

Mr L.L. Dobrin, Chadwick-Helmuth Company, 4601 North Arden Drive, El Monte, California 91731, USA.

SPARES (5 copies)

Total number of copies: **71**

DEFENCE SCIENCE AND TECHNOLOGY ORGANISATION
DOCUMENT CONTROL DATA

1. PRIVACY MARKING/CAVEAT (OF DOCUMENT)

2. TITLE

Synchronous Averaging of Helicopter Tail Rotor Gearbox Vibration: Phase Reference Considerations

3. SECURITY CLASSIFICATION (FOR UNCLASSIFIED REPORTS THAT ARE LIMITED RELEASE USE (L) NEXT TO DOCUMENT CLASSIFICATION)

Document	(U)
Title	(U)
Abstract	(U)

4. AUTHOR(S)

D.M. Blunt

5. CORPORATE AUTHOR

Aeronautical and Maritime Research Laboratory
PO Box 4331
Melbourne Vic 3001 Australia

6a. DSTO NUMBER	6b. AR NUMBER	6c. TYPE OF REPORT	7. DOCUMENT DATE
DSTO-TR-0739	AR-010-666	Technical Report	October 1998

8. FILE NUMBER	9. TASK NUMBER	10. TASK SPONSOR	11. NO. OF PAGES	12. NO. OF REFERENCES
M1/9/411	NAV98/094	DGTA	49	4

13. DOWNGRADING/DELIMITING INSTRUCTIONS

Not applicable.

14. RELEASE AUTHORITY

Chief, Airframes and Engines Division

15. SECONDARY RELEASE STATEMENT OF THIS DOCUMENT

Approved for public release

OVERSEAS ENQUIRIES OUTSIDE STATED LIMITATIONS SHOULD BE REFERRED THROUGH DOCUMENT EXCHANGE CENTRE, DIS NETWORK OFFICE, DEPT OF DEFENCE, CAMPBELL PARK OFFICES, CANBERRA ACT 2600

16. DELIBERATE ANNOUNCEMENT

No Limitations

17. CASUAL ANNOUNCEMENT Yes

18. DEFTEST DESCRIPTORS

Black Hawk helicopters; Military helicopters; Tail helicopter rotors; Tail rotors; Gearboxes; Vibration; Tachometers;

19. ABSTRACT

Synchronous averaging requires an accurate phase reference (tachometer) signal. In helicopter transmissions, such a signal can usually be obtained or derived from an engine or main rotor gearbox accessory, but is not as readily available for the tail rotor gearbox. This report examines whether a separate tail rotor gearbox phase reference signal is necessary by investigating the relative jitter, due to dynamic tail drive shaft twist, between phase reference signals obtained from the main and tail rotor gearboxes in a S-70A-9 Black Hawk helicopter.